AGU PUBLICATIONS

Journal of Advances in Modeling Earth Systems

RESEARCH ARTICLE

10.1002/2017MS000933

Description and evaluation of the Earth System Regional Climate Model (Reg CM-ES)

L. E. Sitz[1,2,3], F. Di Sante[1], R. Farneti[1], R. Fuentes-Franco[1,4], E. Coppola[1], L. Mariotti[2], M. Reale[1,2], G. Sannino[5], M. Barreiro[6], R. Nogherotto[1], G. Giuliani[1], G. Graffino[1], C. Solidoro[2], G. Cossarini[2], and F. Giorgi[1]

[1]Earth System Physics Section, The Abdus Salam International Centre for Theoretical Physics, Trieste, Italy, [2]Istituto Nazionale di Oceanografia e di Geofisica Sperimentale (OGS), Trieste, Italy, [3]Universidad Nacional del Sur, Bahia Blanca, Argentina, [4]Rossby Centre, Swedish Meteorological and Hydrological Institute, Norrkoping, Sweden, [5]Climate Modeling and Impacts Laboratory, Italian National Agency for New Technologies, Energy and Sustainable Economic Development, Rome, Italy, [6]Universidad de la Republica, Montevideo, Uruguay

Key Points:
- A new Regional Earth System Model (RegCM-ES) successfully simulates climate features in regions where coupled air-sea processes are important
- RegCM-ES shows reduction of precipitation biases and good performance simulating the effects of air-sea interactions over frontal regions
- RegCM-ES is an open source community model, making it suitable for use by a large scientific community on any regional domain of interest

Correspondence to:
R. Farneti,
rfarneti@ictp.it

Citation:
Sitz, L. E., et al. (2017), Description and evaluation of the Earth System Regional Climate Model (Reg CM-ES), *J. Adv. Model. Earth Syst.*, *9*, 1863–1886, doi:10.1002/2017MS000933.

Received 2 FEB 2017
Accepted 10 JUL 2017
Accepted article online 13 JUL 2017
Published online 8 AUG 2017

Abstract We describe a new, state-of-the-art, Earth System Regional Climate Model (RegCM-ES), which includes the coupling between the atmosphere, ocean, and land surface, as well as a hydrological and ocean biogeochemistry model, with the capability of using a variety of physical parameterizations. The regional coupled model has been implemented and tested over some of the COordinated Regional climate Downscaling Experiment (CORDEX) domains and more regional settings featuring climatically important coupled phenomena. Regional coupled ocean-atmosphere models can be especially useful tools to provide information on the mechanisms of air-sea interactions and feedbacks occurring at fine spatial and temporal scales. RegCM-ES shows a good representation of precipitation and SST fields over the domains tested, as well as realistic simulations of coupled air-sea processes and interactions. The RegCM-ES model, which can be easily implemented over any regional domain of interest, is open source, making it suitable for usage by the broad scientific community.

Plain Language Summary The increasing availability of observational data sets of high temporal and spatial resolution is providing a more complete view of the ocean and atmosphere, revealing strong air-sea coupling processes. In order to obtain an accurate representation and better understanding of the climate system, its variability, and possible future change, the inclusion of all mechanisms of interaction among the different climate components becomes ever more desirable. Regional coupled ocean-atmosphere models can be especially useful tools to provide information on the mechanisms of air-sea interactions and feedback occurring at regional fine spatial and temporal scales. Here we present a new, state-of-the-art, Earth System Regional Climate Model (RegCM-ES).

1. Introduction

The representation of many important components of the climate system (including the atmosphere, land, ocean, and their interactions) is fundamental for understanding climate variability and change at a wide range of temporal and spatial scales. Satellite remote sensing data of high temporal and spatial resolution have become increasingly available, thus providing a new and enhanced view of the global ocean-atmosphere system and of its air-sea coupling processes (see reviews by *Chelton et al.* [2004], *Xie* [2004], and *Small et al.* [2008]). For instance, a significant wind response to SST fronts has been identified in the Gulf Stream region [*Chelton et al.*, 2004], the Brazil/Malvinas system [*Tokinaga et al.*, 2005], and the Agulhas Return Current [*O'Neill et al.*, 2005], to name a few.

Coupled ocean-atmosphere models are thus essential tools to properly represent air-sea interactions and feedbacks. In the last years, global coupled models have progressively refined their horizontal resolution to attempt to resolve smaller-scale processes. However, fine-resolution regional coupled ocean-atmosphere models, when properly driven by the large-scale circulation, can provide additional information on the

mechanisms of air-sea interactions involving oceanic mesoscale and submesoscale eddies [*Seo et al*., 2006], and can do this at a cheaper computational cost.

Coupled Earth System Models (ESMs) include physical components (i.e., the atmosphere, ocean, land surface, sea-ice) as well as the representation of carbon pathways through the land, atmosphere, and ocean. Due to their extensive computational and storage requirements, global circulation models and ESMs are generally not suited for regional applications requiring high spatial and temporal resolutions and more detailed representation of local processes, features (i.e., topography) and feedback mechanisms. To that end, Regional Earth System Models (RESMs), of different complexity and including a variety of components of the climate system, have been developed and are increasingly used in the study of regional climate variability and change [*Misra et al*., 2009; *Sein et al*., 2015; *Xu and Xu*, 2015; *Byrne et al*., 2016; *Kilpatrick et al*., 2016; *Seo et al*., 2016; *Turuncoglu and Sannino*, 2016].

In this paper, we introduce and publicly release the first version of the Earth System Regional Climate Model (RegCM-ES), which is a state-of-the-art regional coupled model that builds on the RegCM modeling system presented in *Giorgi et al*. [2012] and on previous efforts toward a regional coupled model [*Artale et al*., 2010]. Thanks to its flexibility and modularity, RegCM-ES currently supports the coupling between the atmosphere, ocean, and land surface components, and includes hydrological and ocean biogeochemistry models. More interactive and dynamical components will be activated and implemented in the future, such as an ice sheet model, atmospheric chemistry and dynamic vegetation, to name a few. RegCM-ES can be implemented over any region of interest and early versions have already been successfully tested over some of the COordinated Regional climate Downscaling Experiment (CORDEX) and more domains: South Asia [*Ratnam et al*., 2009], the Mediterranean [*Artale et al*., 2010; *Turuncoglu and Sannino*, 2016], and the Caspian Sea [*Turuncoglu et al*., 2013]. CORDEX is a WCRP-sponsored program that organizes an international coordinated framework to produce an improved generation of regional climate change projections worldwide for input into impact and adaptation studies [*Giorgi et al*., 2009]. RegCM-ES will complement and add value to CORDEX simulations, making it possible for a wider community to be able to perform coupled experiments, from process studies to both hindcasts and future climate scenarios, to answer a wide range of scientific questions.

The RegCM-ES is open source and available under the GNU General Public License (version 3), making it suitable for usage by the large scientific community. Source codes for the driver are distributed through the public code repository hosted on GitHub (https://github.com/uturuncoglu/RegESM). The development of the driver is a collaborative work between the Istanbul Technical University (ITU), the Italian National Agency for New Technologies, Energy and Sustainable Economic Development (ENEA), and the Abdus Salam International Centre for Theoretical Physics (ICTP) [see also *Turuncoglu and Sannino*, 2016]. The RegCM-ES source code also includes the required code patches for the individual model components to be used within the coupled modeling framework. The ICTP's RegCM atmospheric model is also distributed along with the RegCM-ES driver together with all necessary modifications for its coupling. On the other hand, the source codes of the remaining individual model components are distributed by their own official releases, and different licensing types might apply.

In addition to briefly describing the model components and coupling processes, this paper presents three illustrative applications of the coupled model to a Central America and South Atlantic domain and to the tropical band configuration described by *Coppola et al*. [2011]. These applications are not intended to provide a full assessment of the model, but more simply to illustrate its basic physical functioning. The article is organized as follows. In section 2, we describe the individual model components, their coupling and the driver philosophy. In section 3, we analyze the RegCM-ES simulations over the three selected domains. Section 4 highlights some ongoing developments and section 5 presents a summary of our results and future outlooks.

2. The RegCM-ES Model: Individual Components and Coupling

2.1. Atmospheric and Land Surface Component: The RegCM4 Model

The atmospheric component of the regional coupled model is the Regional Climate Model version 4 (RegCM4) [*Giorgi et al*., 2012]. The dynamical core of RegCM4 is based on the primitive equations, hydrostatic version of the National Centre for Atmospheric Research (NCAR) and Pennsylvania State University mesoscale model MM5 [*Grell et al*., 1994]. RegCM4 is maintained by ICTP's Earth System Physics (ESP) section. It can be applied to any region of the world, with grid spacing of up to about 10 km (in the hydrostatic

limit), and for a wide range of studies, from process and model development studies to regional paleoclimate and future climate simulations. A nonhydrostatic version of the model is also currently being tested. RegCM4 is a free software under the terms of the GNU General Public License as published by the Free Software Foundation and as such the code can be downloaded from its own repository (http://gforge.ictp.it/gf/project/regcm/).

RegCM4 includes a range of physical parameterizations for cumulus convection, resolvable scale precipitation and cloud microphysics, planetary boundary layer and radiative transfer processes, which are described in *Giorgi et al*. [2012] and *Nogherotto et al*. [2016]. The performance of different parameterization schemes varies over different domains and climate regimes. We therefore carry out a set of sensitivity experiments with different schemes over each domain to identify the best performing one based on a range of performance metrics. We then use the best performing scheme for each domain. If necessary, we also carry out analogous sensitivity experiments changing the values of parameters within a scheme to optimize the model performance.

To provide a comparison of the large-scale effects with both atmosphere-only and coupled simulations, RegCM4 was tested using two different cloud schemes. In one experiment, the resolvable scale precipitation scheme of *Pal et al*. [2000] is used (Subgrid Explicit Moisture Scheme, SUBEX experiment), whereas a second experiment employs a detailed cloud microphysics scheme (NT experiment) [*Nogherotto et al*., 2016]. In general, the performance of the physics schemes can depend on the region of application, so that different schemes can be selected over different domains (see following sections for more details on our test cases). The model also includes different physical parameterizations of air-sea exchanges of momentum, heat and water vapor, however in the present version of RegCM-ES the only scheme available to describe exchanges with a coupled ocean component is the Zeng Ocean Air-Sea Parameterization [*Zeng et al*., 1998]. A lateral buffer zone is implemented, has a width of 15 grid points in each domain, and the exponential relaxation procedure described in *Giorgi et al*. [1993] is used to provide the model with lateral boundary conditions.

All RegCM4 capabilities are preserved in the coupled RegCM-ES model. Moreover, the flexible design of the coupling interface also supports the use of a one-dimensional lake model [*Hostetler et al*., 1993; *Small et al*., 1999] along with a slab ocean model [*Solmon et al*., 2015]. The driver and coupling interface are designed to adapt easily to future versions and developments of RegCM.

All the experiments presented in this paper employ the Community Land Model 4.5 (CLM4.5) [*Oleson et al*., 2010] for the representation of land surface processes. CLM4.5 is a land surface package which includes soil, vegetation, snow, carbon and nitrogen cycle, and hydrology calculations. It has options to describe dynamic vegetation processes responding to varying climate forcing as well as agricultural and urban environments. In addition, the atmosphere model can use the Biosphere-Atmosphere Transfer Scheme (BATS) [*Dickinson et al*., 1993], which is a much simpler land surface model.

To simulate lateral freshwater fluxes at the land surface and to provide a river discharge to the ocean model, RegCM-ES uses the Hydrological Discharge (HD, version 1.0.2) model developed by the Max Planck Institute [*Hagemann and Dümenil*, 1998, 2001]. The model is designed to run on a fixed global regular grid of 0.5° horizontal resolution, and it uses a pre-computed river channel network to simulate the horizontal transport of water within model watersheds. To do so, different flow processes are used, such as overland flow, base flow, and river flow.

2.2. Oceanic Component: The MITgcm Model

The ocean component of the RegCM-ES is the Massachusetts Institute of Technology General Circulation Model version c63s (MITgcm) [*Marshall et al*., 1997; http://mitgcm.org/]. The MITgcm solves the incompressible Navier-Stokes equations on different types of grid in hydrostatic or nonhydrostatic mode, using finite volume methods and orthogonal curvilinear coordinates in the horizontal. MITgcm has a large user community and has been used for a variety of purposes, from idealized process studies to regional and global ocean simulations [e.g., *Stammer et al*., 2003; *Sannino et al*., 2009; *Furue et al*., 2015; *Rosso et al*., 2015; *Sannino et al*., 2015; *Reale et al*., 2016]. Similar to the atmospheric model component, the ocean model has been modified in order to exchange fluxes with the other components through a driver.

The ocean component can be set to exchange different fields with the overlying atmosphere, depending on the application and the particular setup of the experiment. Air-sea exchange fields are selected from a

predefined field table. For example, the ocean model can be set to use fluxes (heat, freshwater, and momentum) provided by the atmospheric component. Alternatively, it can receive the atmospheric conditions as input, such as surface air temperature, humidity, surface pressure, winds, and precipitation, and compute fluxes internally through bulk formulas. In the configurations presented here, RegCM-ES uses the latter option. Currently, in RegCM-ES, there is no implementation of the interaction between a surface wave model and the ocean, which could be potentially of interest for application in coastal areas. Future releases will address this issue by implementing a wave model within the MITgcm.

In order to use the MITgcm in a regional ocean configuration, we use lateral open boundary conditions prescribed by the MITgcm Open Boundary ConditionS (OBCS) package. (See the on-line MITgcm documentation at http://mitgcm.org/public/r2_manual/latest/online_documents/manual.html.) The geographical definition of OBCS is domain-dependent, and boundary conditions are prescribed using temperature, salinity, and velocity fields which are read from an external file during the runtime. To ensure numerical stability a sponge layer is added to each open boundary of the domain. Each variable is then relaxed toward the boundary values with a relaxation timescale that decreases linearly with distance from the boundary. In our configurations, the thickness of the sponge layer is 1° and inner fields are relaxed toward boundary values with a 10 day period. Details on parameterizations, parameter settings, ocean resolution, and initial and lateral boundary conditions are provided later for each test case study.

2.3. The Driver

To achieve a modular and flexible modeling system that aims to support multiple model components and applications, the RegCM-ES uses the driver based coupling approach developed in *Turuncoglu and Sannino* [2016], an improved version of the original two-component coupled system implemented in *Turuncoglu et al*. [2013]. The coupled model is schematically depicted in Figure 1. The driver couples, controls, and synchronizes each individual model component, interchanging output and input fields, and performing interpolations when necessary.

The driver combines each model component by using its standardized application programming interfaces (APIs). Data exchanges and online regridding capabilities are performed by using the Earth System

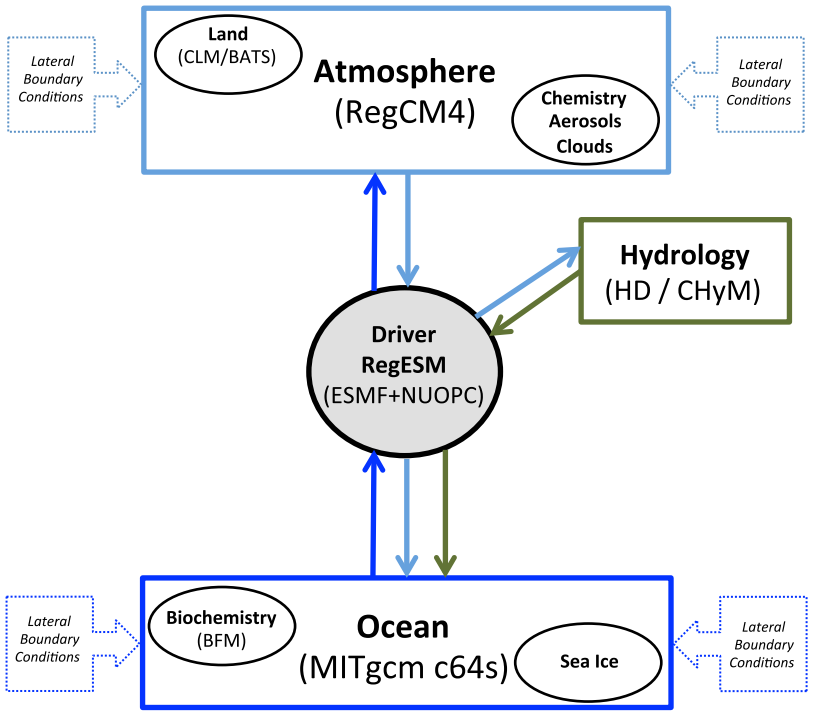

Figure 1. Schematic view of all RegCM-ES modeling components. The arrows indicate the interaction direction between individual components. Both atmosphere and ocean are forced by lateral boundary conditions.

Modeling Framework (ESMF) [*Hill et al*., 2004a, 2004b; *Collins et al*., 2005] and the National United Operational Prediction Capability (NUOPC) layer. Each model component is merged using the latest version of ESMF (version 7.0.0). The ESMF framework is selected because of its online regridding capabilities, which allow the driver to readily perform different types of interpolation (e.g., bilinear, conservative) for the exchange fields. The NUOPC layer simplifies common tasks of model coupling, component synchronization and run sequence by providing an additional wrapper layer between the coupled model and the ESMF framework.

NUOPC also allows the definition of different coupling time intervals among the components. For example, simulations analyzed in this paper have three active components: the atmosphere (ATM), the ocean (OCN), and the river component (HYD). HYD runs on a daily time step and the interaction between the ATM and HYD, as well as HYD and OCN, uses this slow timescale. Instead, ATM and OCN interact with a much higher frequency (3 h for our standard setup).

2.4. Performance and Scalability

The performance tests presented in this section can illustrate potential pitfalls, bottlenecks, and overall scalability limits. The performance benchmarks include analyses of coupling time step frequency and number of components with respect to the total performance and scalability of the coupled model. To reveal the overhead of the coupling, or simply the driver, first each individual model component was tested in standalone mode and then the best performing model configuration was used in the coupled model configuration.

For the sensitivity tests, we used the Central America domain and run several experiments lasting 5 model days (for details on the configuration of the domain see section 3.1). Figure 2 shows the benchmark results, including total wall-clock time and relative speed-up based on 36 cores, for the standalone atmosphere (ATM), the standalone ocean (OCN), and coupled model configurations.

The SUBEX scheme is faster regardless of the number of processors used, but both the SUBEX and NT schemes produce similar ATM scalabilities (Figure 2a). The OCN run is between 1.6 and 2.4 times slower than the ATM-SUBEX configuration, whereas CPL is 2.2–3.4 times slower than ATM. Both OCN and CPL runs reduce their performances in comparison with ATM as the number of cores increases. The NT scheme performance in the CPL run weakens much faster than SUBEX, which shows a better scalability (Figure 2a). In the current setup, the CPL model does not produce significant speed-ups past 250 cores, either using the SUBEX or the NT schemes. In order to assess the driver performance, we tested the coupled model by either using different coupling frequencies, 1 and 3 h (Figure 2d), or by modifying the number of active components (ATM-OCN and ATM-OCN-HYD, Figure 2e). As expected, increasing the frequency of the coupling decreases the performance of the model and its speed-up in sequential mode. However, if the number of cores is higher than 300 both experiments have the same scalability. Adding another component, in this case the hydrological river discharge (HYD), reduces the model performance substantially starting from 72 cores (Figure 2e). Also, as the number of cores increases past 180, the model performance begins to decrease due to higher time consumed for the communication between the various components of the system.

In general, it should be stressed that these performance results may depend on the number of grid points in the domain, with increasing scalability at larger grid point numbers.

3. Testing RegCM-ES Over Selected Domains

In this section, we present illustrative examples of the RegCM-ES performance over three selected regional domains: Central America, South Atlantic, and the Tropical Band. A summary of the main parameters and setup for the three simulations is given in Table 1. Similar experiments were performed for the Indian and Mediterranean CORDEX domains (see Figure 3), and will be described more extensively in separate studies. As RegCM-ES can be used over any regional domain, we anticipate that many more configurations, including but not limited to CORDEX domains, will be tested in the future. After a general assessment of the RegCM-ES performance over the selected domains, some examples on how RegCM-ES represents coupled processes and air-sea interactions will also be given.

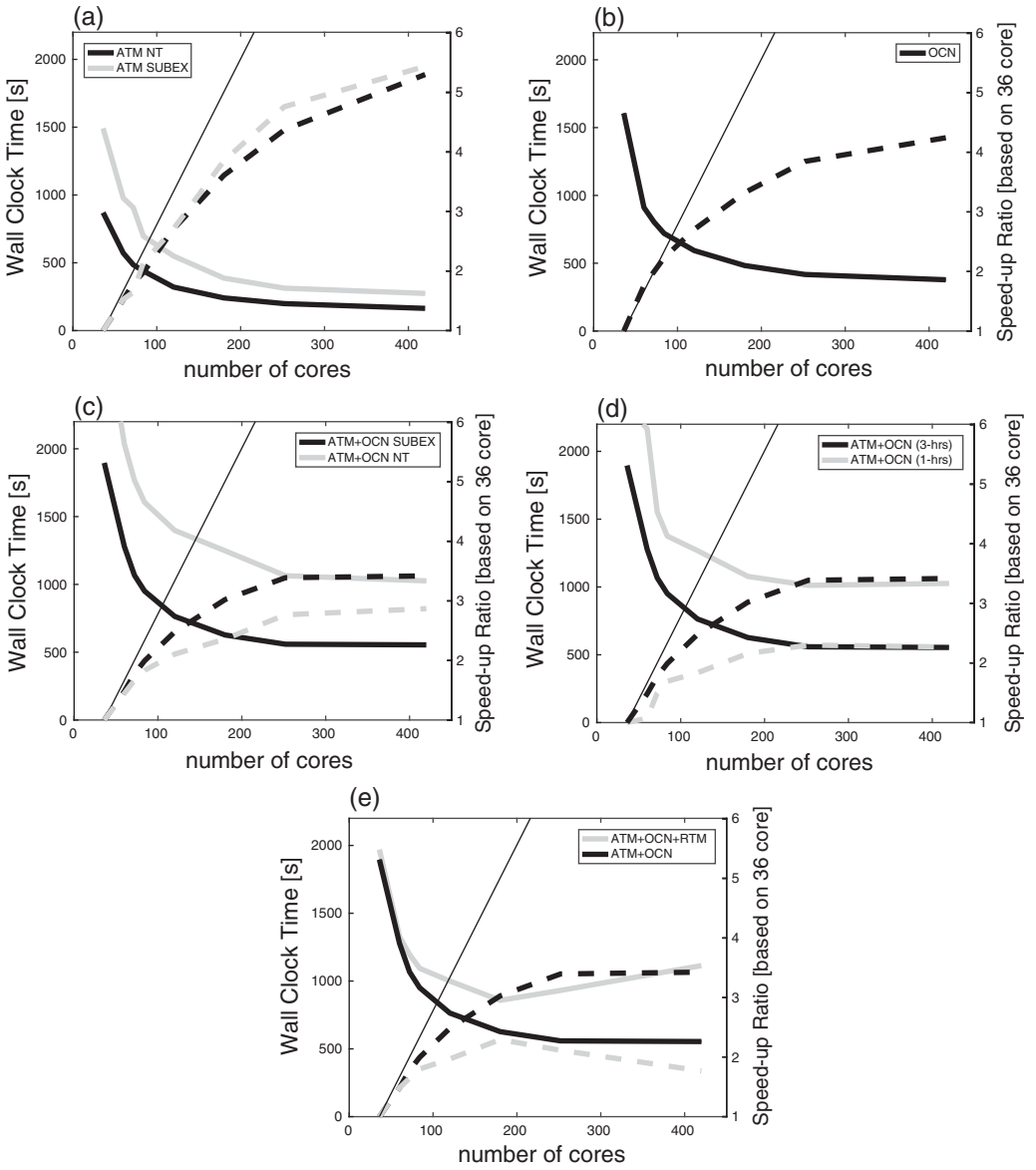

Figure 2. Benchmark results of (a) standalone atmosphere model ATM, (b) ocean only model OCN, and (c) coupled model ATM + OCN. Black lines represent results using the SUBEX scheme, whereas gray lines show model performances using the NT scheme. (d) Effect of coupling interval with a frequency of 3 h (black lines) and 1 h (gray lines), and (e) comparison between simulations using two (ATM + OCN, black lines) or three (ATM + OCN + HYD, gray lines) components in RegCM-ES. Both wall-clock time (left vertical axis, solid lines) and speed-up based on 36 cores (right vertical axis, dotted lines) are shown. In all plots, the thin solid line represents the ideal speed-up.

3.1. The Central American Domain

The atmospheric domain over Central America (CA) follows the CORDEX specifications, covering a large area of Central America and adjacent ocean and land regions at a grid spacing of 50 km and 23 vertical sigma/p levels. The atmospheric component employs an enhanced radiative transfer scheme [*Kiehl et al*., 1996; *Giorgi et al*., 2012] and the planetary boundary layer scheme of University of Washington (UW-PBL) [*Bretherton et al*., 2004]. For cumulus convection, we used the scheme of *Tiedtke* [1989] over land and *Emanuel* [1991] over ocean. In addition, both the SUBEX and NT resolvable scale precipitation schemes are tested. All simulations use the ERA Interim reanalysis [*Dee et al*., 2011] as lateral boundary and initial atmospheric conditions.

The ocean model covers the region from 15°S to 54°N and 145°W to 15°W (Figure 3) at a horizontal resolution of ∼0.125° in both zonal and meridional directions. The vertical resolution ranges from 1 m near the

Table 1. Main Oceanic and Atmospheric Setup, Parameters, and Parameterizations for the Experiments Presented in This Study[a]

	Central America	South Atlantic	Tropical Band
Period	1988–1997	1988–1997	1979–2008
Land surface	CLM4.5	CLM4.5	CLM4.5
Hydrology	HD	HD	HD
Atmosphere			
Domain	[17°S–53°N; 148°W–1°W]	[65°S–20°N; 130°W–60°E]	[43°S-43°N]
Horiz. Res.	50 km	50 km	100 km
Vert. Res.	23 levels	23 levels	23 levels
Conv. Land	*Tiedtke* [1989]	*Tiedtke* [1989]	*Tiedtke* [1989]
Conv. Ocean	*Emanuel* [1991]	*Tiedtke* [1989]	*Tiedtke* [1989]
Precip.	SUBEX/NT	SUBEX/NT	NT
BC	ERA-Int	ERA-Int	ERA-Int
IC	ERA-Int	ERA-Int	ERA-Int
Ocean			
Domain	[15°S–54°N; 145°W–15°W]	[54°S–10°N; 70°W–30°E]	[30°S–30°N]
Horiz. Res.	1/8°	1/8°	1/4°
Vert. Res.	40 levels	40 levels	45 levels
BC	MOM025	MOM025	SODA 2.2.4
IC	MOM025	MOM025	SODA 2.2.4

[a]Period simulated (in years); land surface model (CLM4.5) [*Oleson et al.*, 2010]; hydrological discharge model (HD) [*Hagemann and Dümenil*, 1998, 2001]; horizontal resolution (Horiz. Res.); vertical resolution (Vert. Res.); cumulus convection scheme over land and ocean (Conv. Land, Conv. Ocean) which is either *Tiedtke* [1989] or *Emanuel* [1991]; resolvable scale precipitation scheme (Precip.) which is either SUBEX from *Pal et al.* [2000] or NT from *Nogherotto et al.* [2016]; boundary conditions (BC) and initial conditions (IC), which for the atmosphere are taken from ERA Interim reanalysis [*Dee et al.*, 2011] and for the ocean from either a global ocean simulation (MOM025) or SODA reanalysis version 2.2.4 [*Carton and Giese*, 2008].

surface to 250 m near the bottom with a total of 40 z-levels. The model uses the nonlinear free surface, a nonslip condition at the land boundaries and a quadratic form of bottom friction with a drag coefficient of 0.002. Vertical mixing is parameterized with the K-profile parameterization of *Large et al.* [1994], while the Smagorinsky scheme [*Smagorinsky*, 1993] is implemented for viscosities, with a biharmonic coefficient of 3 following *Griffies and Hallberg* [2000]. The background coefficient is set to 1×10^{-5} m^2 s^{-1} for viscosity and 5×10^{-5} m^2 s^{-1} for tracer diffusion. The bathymetry was obtained from the global topography of *Smith and Sandwell* [1997].

Initial and lateral boundary conditions for the regional ocean model were obtained from a global integration of the NOAA/Geophysical Fluid Dynamics Laboratory MOM model at 0.25° horizontal resolution (MOM025; www.mom-ocean.science/web) forced by the interannually varying CORE-II atmospheric state for

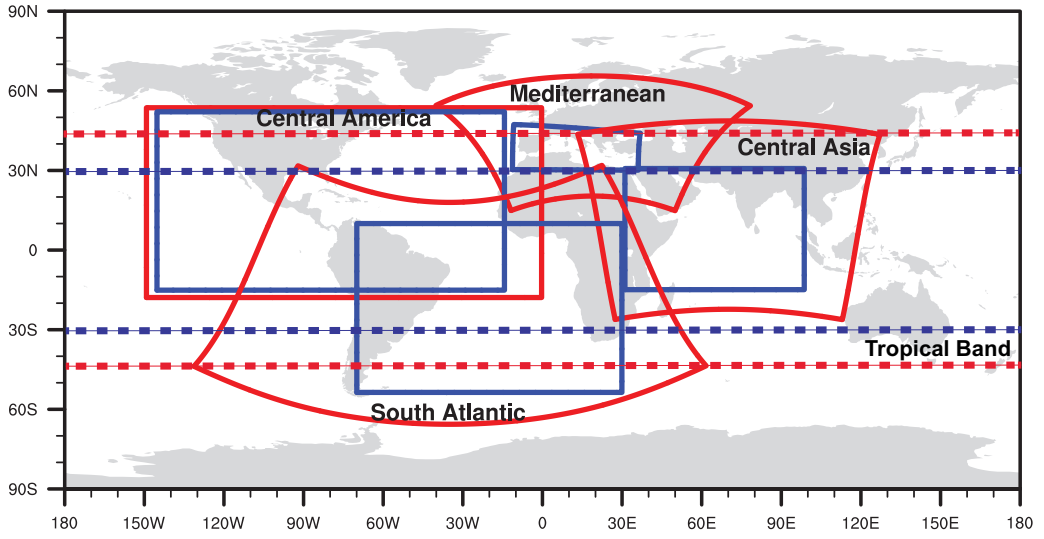

Figure 3. Different domains over which the RegCM-ES model has been tested. The solid red lines indicate the atmospheric model domain. The blue solid box shows the ocean model domain. Dotted lines are for the Tropical Band domain extending to 42° and 30° for the atmosphere and ocean, respectively.

the 1948–2007 period [*Danabasoglu et al*., 2014], after interpolating temperature, salinity, and horizontal velocities onto the model grid. Lateral boundary conditions include temperature, salinity, and velocity components. Sponge layers of 1° are implemented at each boundary, where monthly averaged fields are prescribed every 10 days.

Differences in grid spacing between the global and regional models lead to systematic errors after interpolation, particularly in the case of the velocity fields. To avoid a possible mass imbalance between boundaries, the interpolated normal velocity fields across each open boundary are further individually adjusted to impose the same transport given by the original coarse grid of the global MOM025 model. Adjustments at each boundary are added as a barotropic velocity uniformly distributed over all grid points.

The coupled model RegCM-ES is run for 10 years, from 1988 to 1997, a decade straddling both atmospheric and oceanic boundary conditions. Averaged fields and biases are computed over the entire experimental period. The use of a spin-up, in order to let the ocean model equilibrate particularly in its bottom layers, is still a matter of debate in the regional ocean modeling community. A spin-up is desirable in free-running ocean and coupled models, as these will deviate considerably from the initial oceanic conditions and will tend to drift toward a new state given by the ocean physics and possible interactions with other climate components. However, regional ocean models and in particular regional simulations that aim at performing hindcasts of the recent past might benefit from being in a state as close as possible to the observed. In addition, the use of lateral boundary conditions in a limited ocean domain imposes a relative control on the interior solution. We tested this hypothesis and computed the drift in temperature and salinity both at the surface and bottom during the length of the simulation. Over the 10 year period, the area-averaged temperature (salinity) oscillates around 0.2°C (0.2) at the surface and drifts of ∼0.035°C (∼0.0015) at the bottom (not shown). Moreover, we are imposing lateral boundary conditions derived from a global ocean models, and the interior solution largely reflects small drifts introduced by the global model.

3.1.1. Comparison With Observations: Coupled Versus Standalone

The seasonal precipitation biases for the atmospheric and coupled simulations are shown in Figure 4. As previously reported in *Fuentes-Franco et al*. [2014], all simulations show a prevailing tendency to overestimate rainfall over the topographically complex areas of the domain, particularly during summer, although the overall regional topographically induced spatial details are captured.

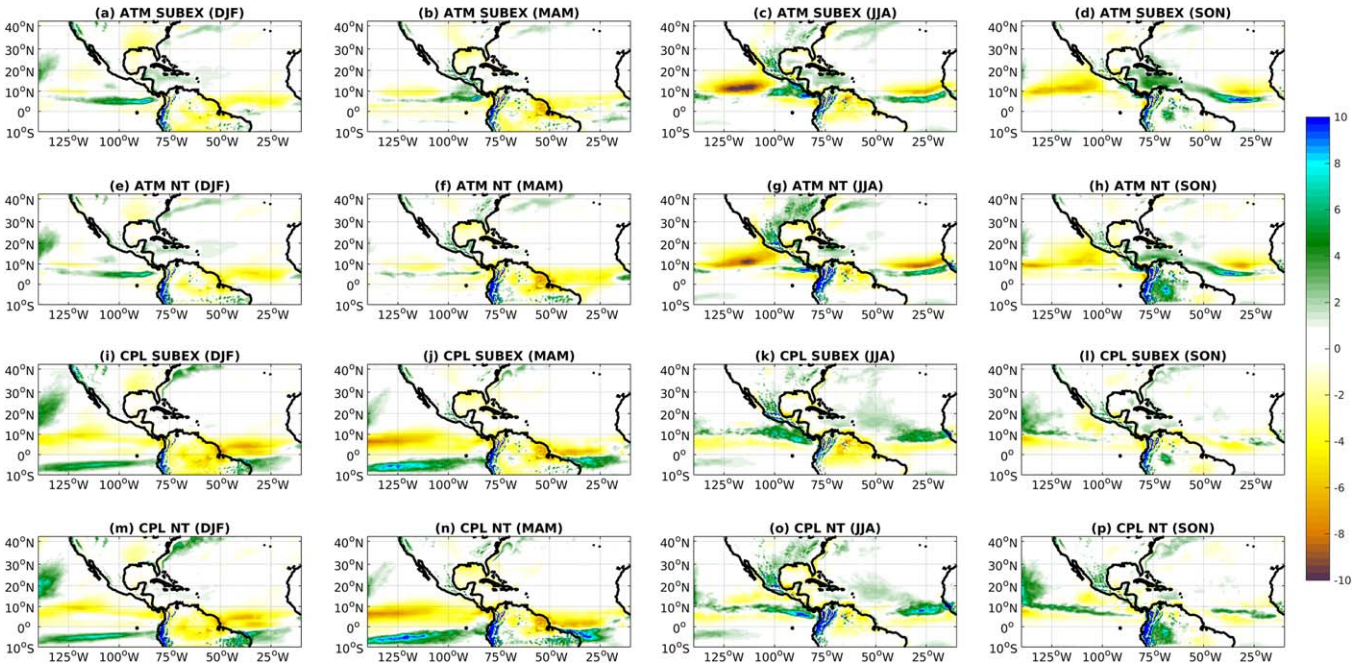

Figure 4. Precipitation bias (in mm d^{-1}) over the Central America domain with respect to observations (GPCP). (a–d) Standalone atmospheric model (ATM) using SUBEX scheme; (e–h) ATM model using NT; (i–l) coupled model (CPL) using SUBEX, and (m–p) CPL with the NT scheme. Biases are computed over the period 1988–1997 of austral summer (DJF, left), autumn (MAM, center left), winter (JJA, center right), and spring (SON, right).

When comparing the results using the SUBEX and NT schemes in the atmosphere-only simulations, the main differences are given by smaller biases over the Eastern Tropical Pacific (ETP) in the NT (Figures 4e–4f versus 4a–4d) in all seasons. In MAM, for example, a slight northeastward shift of the simulated Inter-Tropical Convergence Zone (ITCZ) over the ETP (see Figure 4b) generates a wet bias over the Southwestern Mexican and Central-American coasts in the SUBEX simulation, which is improved by the NT scheme (Figure 4f).

Over land, differences are found over the Northern extension of the Andes where the NT shows an overestimation of precipitation compared to SUBEX. However, in general, the NT scheme shows some improvements in the dry bias found in SUBEX over Northern South America, producing a wet bias in SON. Similarly, over North America the NT scheme shows smaller dry biases over the South and Midwest USA compared to SUBEX.

The coupled simulations using the NT and SUBEX schemes show similar changes compared to the corresponding atmosphere-only simulations. The coupled simulations (Figures 4i–4p) yield an improvement of the biases over the Tropical North Atlantic (TNA) by reducing the wet bias over the Caribbean Sea found in the atmospheric only simulations. Furthermore, the location of the ITCZ over the TNA is improved in the coupled simulations, especially in the rainy season (JJA and SON), since the atmosphere-only simulations show a southern shift of the ITCZ position. Over the ETP, in DJF and MAM, there is a shift of the ITCZ toward the south, with wet anomalies at latitudes south of the Equator. However, in JJA and SON, the dry bias present in the atmosphere-only simulations over the northern ETP (from 10°N to 20°N and from 130°W to 100°W) is strongly reduced in the coupled simulations (Figures 4c, 4d, 4g, 4h, 4k, 4l, 4o, and 4p).

Precipitation biases can be partially explained by the SST biases in the coupled simulations shown in Figure 5. In all seasons, the SST over the TNA presents warm anomalies in the easternmost part of the domain, and cold anomalies in its westernmost parts along the South American coast and the Caribbean Sea. The warmer than observed SST over the eastern TNA (Figures 5c and 5d) causes intensified convection that is responsible for the wet bias during JJA and SON (Figures 4k and 4l). Conversely, over the ETP, there is a warm anomaly in the northernmost regions along the US and Baja California coast and South of the Equator in the region Niño 1 + 2 (0–10°S; 90–80°W). This warm bias causes a southern shift of the ITCZ Figures 4i, 4j, 4m, and 4n, which is in fact intensified in DJF and MAM, when a cold bias in the central Pacific extends east toward the coasts of Mexico and Central America. During the warm period of the year (JJA and SON), there is a warm SST bias throughout the ETP, except over the Equator.

Over land, coupled simulations do not show significant changes compared to the corresponding atmosphere-only simulations. However, an added value of the NT scheme versus the SUBEX scheme is found over the ETP close to the Central American coasts (Figures 4k and 4o, respectively), where an improvement of the wet biases is found in JJA, despite the presence of a warmer SST bias in the NT region (Figure 5g) compared to SUBEX (Figure 5c).

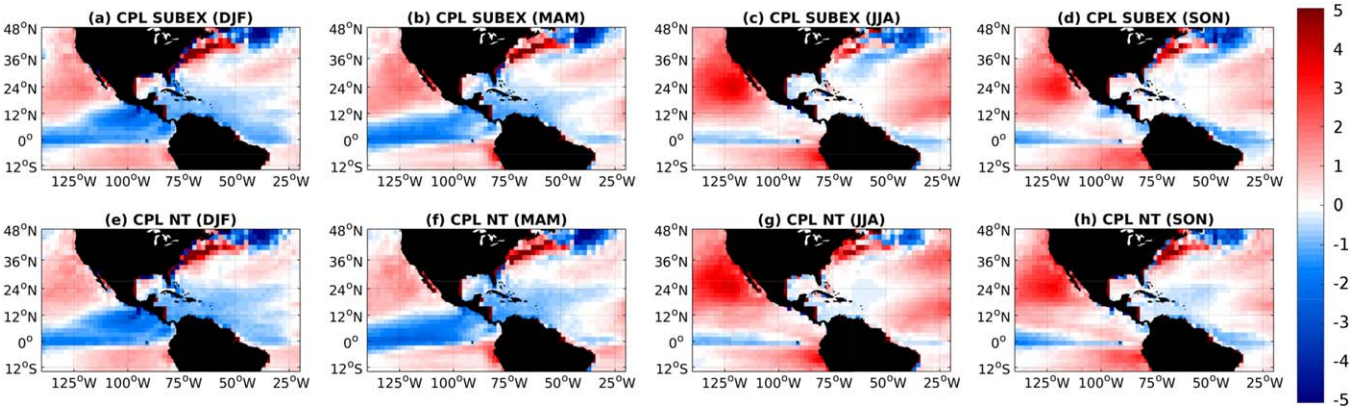

Figure 5. Sea surface temperature (SST, in °C) bias over the Central America domain with respect to NOAA NCDC ERSST version 4. (top) SUBEX experiment and (bottom) using the NT scheme. Biases are computed over the period 1988–1997 of austral summer (DJF, left), autumn (MAM, center left), winter (JJA, center right), and spring (SON, right).

3.1.2. Tropical Pacific Ocean and Atlantic Transports

Achieving a realistic representation of subsurface properties in the Tropical Pacific is fundamental for a proper simulation of coupled ocean-atmosphere processes, such as the El Niño Southern Oscillations (ENSO). The Tropical Pacific upper ocean state is controlled by a delicate balance between surface forcing, mainly wind stress, and ocean physics such as vertical mixing and lateral friction. Hence, in a coupled framework, both atmospheric and oceanic conditions will influence the structure of the upper Pacific Ocean.

Figure 6 shows the equatorial upper ocean temperature and zonal velocity from the SODA [*Carton and Giese*, 2008] reanalysis product and RegCM-ES averaged over the years 1988–1997. The model maintains a thermocline which is in good agreement with the reanalysis, especially in the eastern Pacific where many models have difficulties in reproducing the observed thermal stratification [*Griffies et al*., 2009] due to lack of oceanic and atmospheric resolution. The thermocline is shown to be too diffusive in the model, although stratification below the thermocline is well represented between 11°C and 14°C. Equatorial zonal currents also show comparable strengths in RegCM-ES and SODA, with the equatorial undercurrent peaking at 1.1 m s^{-1} as in SODA, although its core is deeper than observed. Surface currents are overestimated, possibly due to stronger and too-westward wind stresses, causing a cold bias around the center of the domain.

The Atlantic side of the Central American domain encompasses a large fraction of the subtropical North Atlantic, the Caribbean Sea, and the Gulf of Mexico. The last two regions require fine horizontal and vertical resolution in order to simulate oceanic transports through narrow and shallow straits and account for

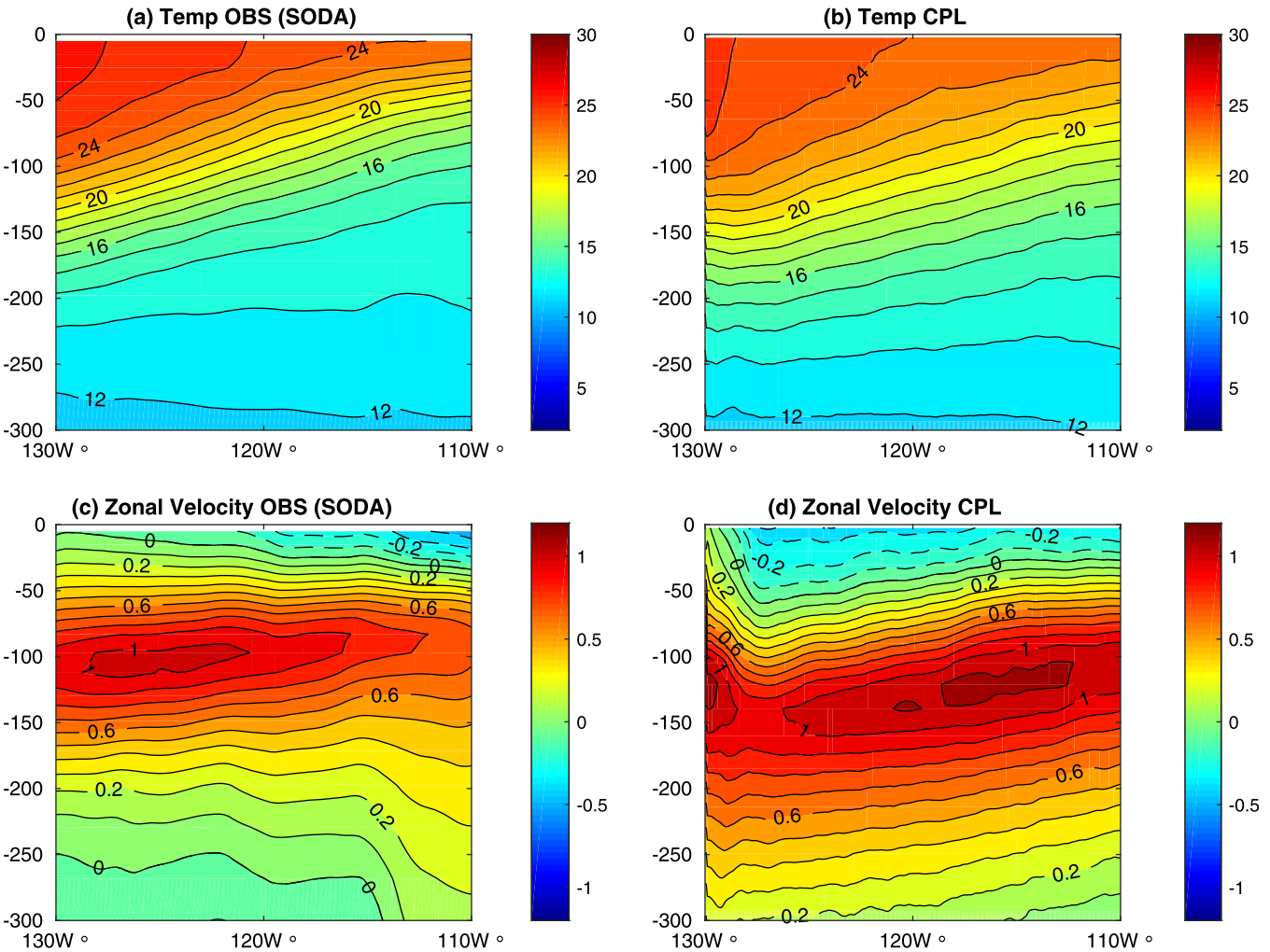

Figure 6. (top) Upper ocean temperature (in °C) at the equator in the Pacific Ocean. (bottom) Upper ocean zonal velocity component (in m s^{-1}) at the equator in the Pacific Ocean. Time-mean values over the period 1990–1995 are shown for (left) reanalysis temperatures (SODA) and (right) RegCM-ES.

intense air-sea interactions in what is commonly defined the Atlantic warm pool [*Misra et al*., 2009]. A common evaluation for ocean models is the estimation of volume transports through well-measured "choke points" (straits or passages) which are known to be a measure for the fidelity of the simulated large-scale circulation.

Much of the warm and salty upper limb of the meridional overturning circulation in the North Atlantic enters the Caribbean Sea through the many passages on its eastern flank. These circulations merge and flow through the Yucatan Channel (between Mexico and Cuba) into the Gulf of Mexico and exit through the Florida Strait as the major source of the Gulf Stream. The time-mean flow through the Yucatan channel in RegCM-ES is 29.6 ± 2.7 Sv (1 Sv$\equiv 10^6$ m^3 s^{-1}), very close to the observational estimate of 30.5 ± 5.3 Sv [*Rousset and Beal*, 2010]. In contrast, the global model MOM025 has a weaker transport of 22.8 Sv. The sluggish Yucatan transport in MOM025 can largely be explained by the weak Windward Passage transport (between the islands of Cuba and Hispaniola) of 1.9 Sv, which is observed to be 7.5 ± 1.6 [*Smith*, 2010] and is 8.4 Sv in the fine-resolution RegCM-ES. As a consequence, the Florida Strait transport in RegCM-ES is 31.6 ± 2.2 Sv, closely matching the observation of 30.8 ± 3.2 [*Rousset and Beal*, 2011], whereas MOM025 only transports 26.6 ± 4.1 Sv northward through the Florida Strait during the same period. RegCM-ES then better represent transports through the main straits in the Caribbean Sea, with consequences for the injection of warm and salty waters of equatorial origin into the Gulf of Mexico and the resulting intensity of the Gulf Stream.

3.1.3. Air-Sea Interactions in a Tropical Cyclonic Event

Strong winds associated with tropical cyclones (TCs) generate a cooling in SST behind the storm. The cooling has been shown to rely on five different processes: (1) the intense wind stress around the cyclone causes the entrainment of cold water from the underlying thermocline into the ocean mixed layer leading to a decrease in SST [*Leipper*, 1967; *Bender et al*., 1993; *Hart et al*., 2007; *Hart*, 2011; *Price et al*., 2008; *Jansen et al*., 2010]; (2) enhanced surface sensible and latent heat fluxes from the ocean to the atmosphere driven primarily by the high wind speeds near the radius of maximum winds [*Price*, 1981; *Emanuel*, 2001; *Trenberth and Fasullo*, 2007]; (3) horizontal transports of warm water away from the storm center [*Leipper*, 1967]; (4) rain falling onto the ocean surface; and finally (5) radiative losses [*Brand*, 1971]. SST cooling can vary from less than 1°C up to 9°C [*Price*, 1981; *Lin et al*., 2003; *Walker et al*., 2005; *Price et al*., 2008].

According to *Dare and McBride* [2011], following the reduction in SST caused by the TC passage, subsequent atmospheric and oceanic processes tend to restore the SST to the climatological value with a time that varies widely between different TCs, from days to weeks. Larger reductions in SST are associated with more intense TCs and with storms that move slowly. Atmosphere-ocean feedbacks associated with tropical cyclones are important for controlling the duration, intensity, and track of the tropical cyclone, and they can be reproduced in coupled model simulations, where the exchange of mass and energy between the atmosphere and ocean is possible.

An illustrative example is provided in Figure 7, where the track and underlying SST are shown for an observed and a simulated TC event. The observations (Figure 7a) show the 6 h track of the hurricane Gabrielle and corresponding SST (Daily OI-V2) [*Reynolds et al*., 2007] during 1–12 September 1989. Figure 7b shows the forcing SST field (ERA Interim at 0.75° resolution) and a 3 h tracked simulated TC at the end of August 1995 in the atmosphere-only simulation. Similarly, in Figure 7c, we show the simulated SST and two 3 hourly tracks of TCs formed during the same period but in the coupled simulation. The cyclone tracking was performed using *kyklop*, a tracker scheme developed by *Fuentes-Franco et al*. [2016] for high resolution climate models. As in the observations, the coupled simulation produces colder SSTs beneath the TC tracks, which is obviously not found in the atmosphere-only simulation where the SST field is not interacting with the atmosphere above.

Note that, in a climate-mode experiment, simulated cyclone tracks do not necessarily correspond spatially with observed tracks [see *Fuentes-Franco et al*., 2016]. Therefore, Figure 7 only serves as an example of atmosphere-ocean interactions during a TC, without the intention to simulate a particular observed event. A detailed analysis on the properties of the simulated TCs in both the Atlantic and Pacific Oceans, the effect of an SST bias on their genesis and evolution (compare Figures 7a and 7c), as well as an assessment of all air-sea interactions at play will be the subject of a following study.

3.2. The South Atlantic Domain

During summer most of South America is influenced by the monsoon, with the South Atlantic Convergence Zone (SACZ) being a dominant feature in regulating precipitation variability over eastern Brazil and

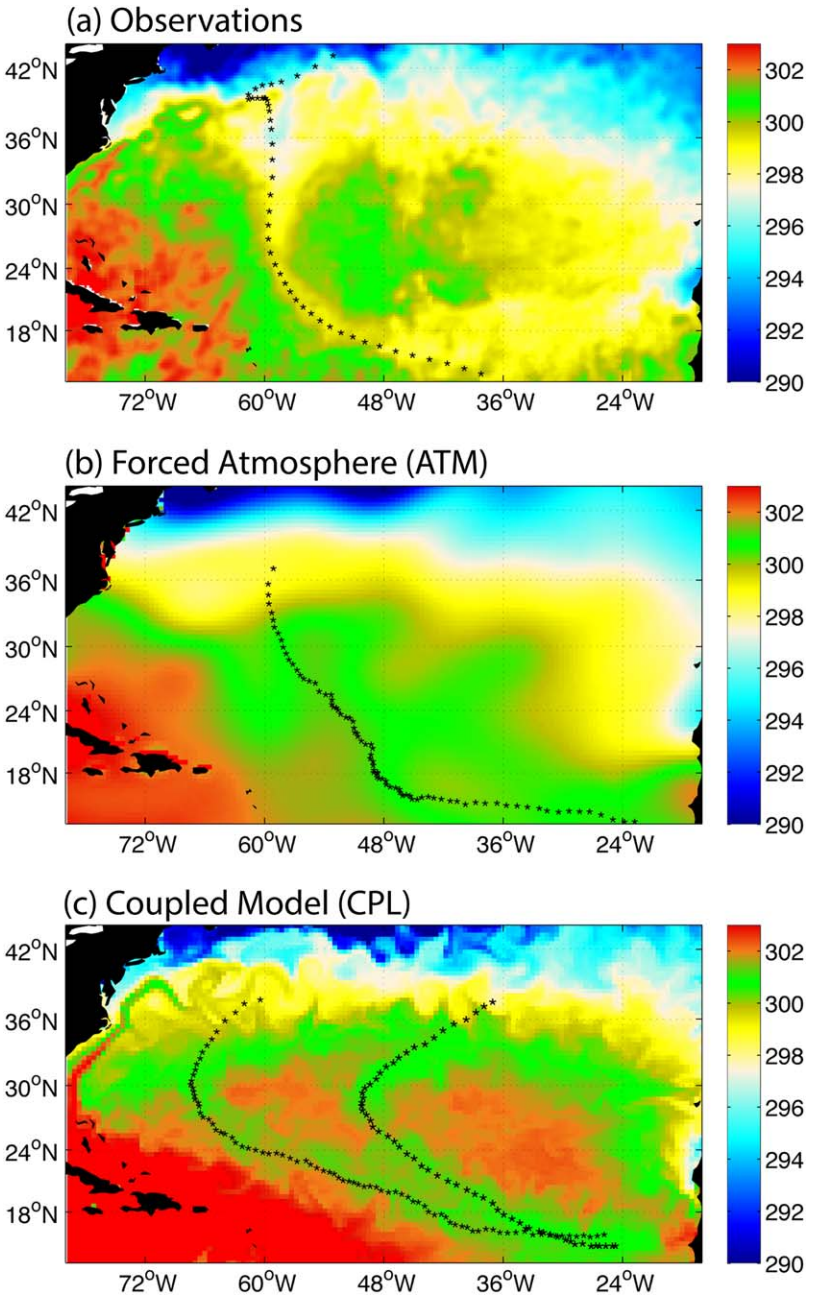

Figure 7. (a) Six hourly track of the hurricane Gabrielle and the underlying SST field (in K) from daily OI-V2 [*Reynolds et al*., 2007]; (b) similar to Figure 7a but for an atmosphere-only simulation (ATM); (c) similar to Figure 7a but for a coupled RegCM-ES simulation (CPL). Numerical simulations do not represent a particular observed event, and the figure illustrates an example of a tropical cyclone simulation and atmosphere-ocean interactions, when present.

Uruguay. The synoptic activity of the SACZ is modulated by upper level Rossby waves that extend from the extratropical Pacific to the northeast over South America. Recently, it was shown that the propagation path of these waves varies among years and as a consequence, the synoptic SACZ activity is also highly variable [*Tirabassi et al*., 2014]. In particular, if the path of the wave bends to the northeast so that circulation anomalies are largest over the continent, rainfall anomalies over land are strongest. On the other hand, if the path is more zonal, rainfall anomalies over land are relatively small, the oceanic extension of the SACZ is strong and anomalies persist longer. This latter effect has been ascribed to the local oceanic forcing of the SACZ. Thus, the dynamics of the SACZ, and its interaction with the local ocean, as well as its predictability depends

on the trajectory of the extratropical transients. Several previous studies have shown the importance of regional air-sea interactions in the interannual variability of the SACZ [e.g., *Barreiro et al*., 2002, 2005].

The South Atlantic region simulated with the present modeling system was designed to allow the representation of the path of the transients associated with the main modes of variability in the SACZ and their dependence on regional air-sea interactions. The atmospheric domain, bounded between 65°S–20°N and 130°W–60°E, uses the Mercator-rotated projection at a grid spacing of 50 km and 23 vertical sigma/p levels. For the convection scheme, we use the one of *Tiedtke* [1989] both over land and ocean. Similarly to the Central American domain, we performed two experiments with either the SUBEX or the NT explicit cloud schemes. Boundary conditions are from ERA Interim reanalysis [*Dee et al*., 2011].

The ocean domain spans from 54°S to 10°N and 70°W to 30°E, and has a horizontal resolution of ∼0.125° in both the zonal and meridional directions. The vertical resolution ranges from 5 m near the surface to 250 m near the bottom, with a total of 40 z-levels. The remaining physical parameterizations are the same as in the Central American domain, and the model is run for the same 10 years period (1988–1997).

3.2.1. Comparison With Observations: Coupled Versus Standalone

Similarly to the results reported in *Reboita et al*. [2014], when using the Tiedke parameterization for cumulus convection, an underestimation of precipitation in the Amazonian region and north of Brazil is found (Figure 8), associated with a lower evapotranspiration reducing the static energy and the fraction of the convective rainfall. This negative precipitation bias is found throughout the year but is higher in MAM and JJA (Figures 8b and 8c). Over the ocean region of the ITCZ, precipitation in the SUBEX experiment is higher than observed, especially south of the Equator near the coast of Brazil, as a result of an ITCZ located too far south (Figures 8a and 8d). In the austral spring, the simulated ITCZ is also stronger than observed.

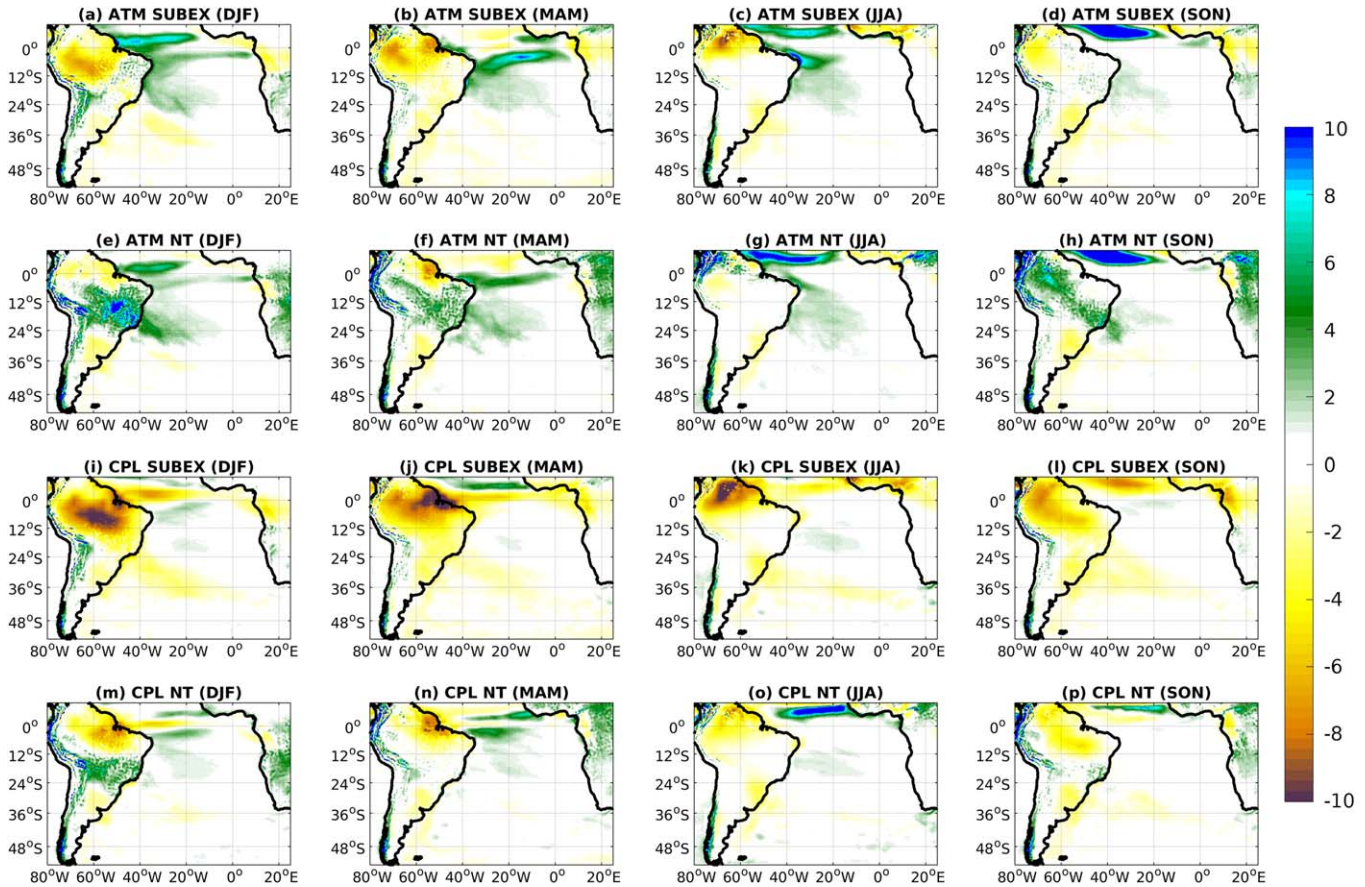

Figure 8. Precipitation bias (in mm d^{-1}) over the South Atlantic domain with respect to observations (GPCP). (a–d) Standalone atmospheric model (ATM) using SUBEX scheme; (e–h) ATM model using NT; (i–l) coupled model (CPL) using SUBEX, and (m–p) CPL with the NT scheme. Biases are computed over the period 1988–1997 of austral summer (DJF, left), autumn (MAM, center left), winter (JJA, center right), and spring (SON, right).

The region denoted by Uruguay, northeast of Argentina, and southern Brazil (the La plata basin) present lower precipitation than observed, with largest negative biases in winter and spring. This deficit in precipitation is a common problem of many RCMs [*Solman et al*., 2013] and also previous versions of the regional atmospheric model [*da Rocha et al*., 2012].

Using the NT scheme in the atmosphere-only simulation, reduces precipitation biases considerably over the northeast coast of Brazil both in DJF and JJA (Figures 8e and 8g). The ITCZ over the ocean is also better represented in summer, although with the NT scheme the positive bias during winter is stronger than in SUBEX (Figures 8a, 8e, 8c, and 8g). Overall, during summer and fall, regions of positive biases over the ocean are lower when using NT. This scheme also improves the precipitation field over the Amazon region and north of Brazil, but overestimates rainfall in the SACZ, particularly over the continent (Figures 8e and 8f). The higher precipitation over land in the NT experiment is due to the fact that the microphysics scheme receives the detrained mass flux from the Tiedke convection scheme and this is assumed to condense into cloud water or into ice diagnostically using a coefficient function of temperature. This process is applied for all types of convection, namely deep, shallow, and midlevel, favoring in particular stratiform precipitation over land, which is underestimated by the SUBEX scheme.

The coupled model shows smaller precipitation biases over the ocean both using the NT and SUBEX schemes (Figures 8i–8l versus 8m–8p). However, with SUBEX the driest regions over land found in the atmosphere-only run become even drier, especially in the Amazon region and the northern part of Brazil during summer (Figure 8i). This is probably connected with the fact that the SST is too low north of 30°S (Figures 9a–9d), reducing the transport of moisture inland and the formation of convective rainfall. Overall, the results of the coupled model using SUBEX in this domain show relatively low precipitation values (Figures 8i–8l).

The implementation of the NT scheme in the coupled model results in the smallest precipitation bias across the domain year round. The biases in the ITCZ seen in atmosphere-only runs are strongly reduced in both the warm and cold seasons. Over South America, however, the negative bias north of 10°S during summer persists (Figure 8m). On the other hand, even if the precipitation over the continental portion of the SACZ is still overestimated, it is approaching observational values (Figure 8e versus 8m). Moreover, the oceanic portion of the SACZ is well simulated, showing no significant bias. Finally, the La Plata basin region presents the lowest precipitation bias when using the coupled model with the NT scheme (Figures 8a, 8e, 8i, versus 8m).

The SST bias in the SUBEX and NT coupled runs partially explain the differences in precipitation between these two experiments (Figure 9). North of 24°S, the NT scheme run has higher SSTs than the SUBEX one. This enhances evaporation and the transport of moisture intensifying convection and favoring precipitation over the SACZ and the Amazon region.

There is a positive SST bias of up to 5°C in both coupled experiments close to the western coast of Africa at around 24°S. This is a typical region that coupled climate models find hardest to simulate well due to the

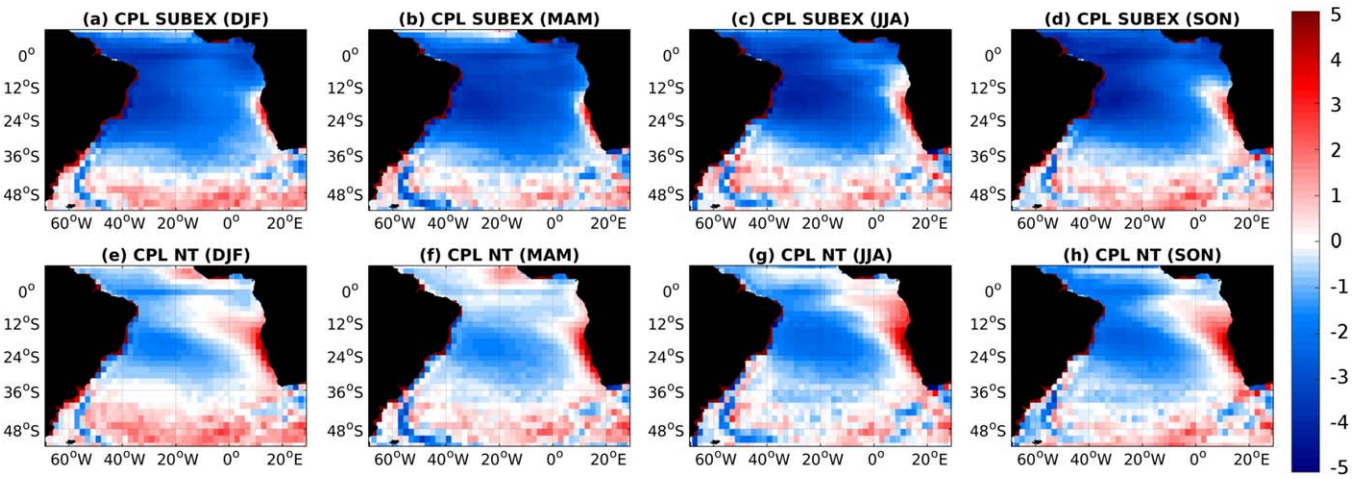

Figure 9. Sea surface temperature (SST, in °C) bias over the South Atlantic domain with respect to NOAA NCDC ERSST version 4. (top) SUBEX experiment and (bottom) using the NT scheme. Biases are computed over the period 1988–1997 of austral summer (DJF, left), autumn (MAM, center left), winter (JJA, center right), and spring (SON, right).

presence of an upwelling system produced by the interaction between the Benguela current, wind stress, and the bathymetry. In a recent study, *Small et al.* [2015] found that, in order to correctly simulate the Benguela upwelling system, the atmospheric circulation has to represent realistically the local wind stress curl at the eastern boundary, which they achieve only with a horizontal resolution of at least 27 km. Therefore, even though the use of the NT scheme reduces the overall SST biases in the basin, in order to correct the positive bias in the Benguela region, the atmospheric resolution should be substantially refined. Sensitivity experiments will be performed in future to address this issue.

3.2.2. Meridional Ocean Transports

Figure 10 shows the annual mean vertical cumulative volume transport (CVT) at 35°S averaged over the period 1988–1997 from RegCM-ES and the ocean global model (MOM025) used to produce the lateral boundary conditions for the regional coupled model. RegCM-ES produces a weaker equatorward transport at intermediate (∼500 to ∼1200 m) layers as well as weaker poleward transport in the deeper layers compared to MOM025. Despite having weaker transports, RegCM-ES better reproduces the depth at which the transport reverses (around 1200 m), as shown by observations [*Dong et al.*, 2009]. In the bottom layers, both models capture the northward transport associated with the presence of Antarctic Bottom Waters. Because of a bias in the lower densities, the northward bottom transport in MOM025 is found below 4200 m, whereas the transport in RegCM-ES is located at the same depth as in the observations [*Dong et al.*, 2009].

The time-mean value of the South Atlantic Meridional Overturning Circulation (SAMOC) [*Sitz et al.*, 2015] index in RegCM-ES, defined as the maximum of the zonally integrated northward CVT from surface to bottom across 35°S is 11.01 ± 3.08 Sv, somewhat weaker than recent observational and modeling estimates (17.9 ± 2.2 Sv [*Dong et al.*, 2009], 15 ± 3.7 Sv [*Dong et al.*, 2011], 15.6 ± 3.1 Sv [*Perez et al.*, 2011], 10.28 ± 1.37 Sv, 12.01 ± 1.42 Sv, 14.72 ± 1.26 Sv [*Sitz et al.*, 2015]). The total time-mean volume transport through 35°S is −1.08 ± 0.6 Sv, which is also in the range of previous reported estimates of ∼0.5 Sv [*Baringer and Garzoli*, 2007], ∼0.6 Sv [*Dong et al.*, 2011], ∼0.77 Sv [*Sloyan and Rintoul*, 2001], and ∼1 Sv [*Talley*, 2008].

RegCM-ES thus properly represents South Atlantic oceanic meridional fluxes, subject to lateral boundary conditions derived from a global model integration. Future experiments with different products imposed at the boundaries such as ocean reanalyses, along with changes to model physics, will test the sensitivity of the representation of meridional ocean transports.

3.2.3. Eddy Kinetic Energy and Air-Sea Interactions Over Ocean Frontal Systems

Mesoscale ocean eddies, with a typical latitude-dependent length scale of 10–100 km, interact with the atmosphere, potentially modifying the marine atmospheric boundary layer (MABL) and wind stress through SST and surface current anomalies [*Xie*, 2004; *Chelton and Xie*, 2010; *O'Neill et al.*, 2010, 2012]. Using a fine-resolution coupled model, *Seo et al.* [2016] found that in the California Current Systems, in regions of intense mesoscale energy activity, surface eddy kinetic energy (EKE) is weakened almost entirely by the effect of surface currents on wind stress. On the other hand, when eddies are embedded in a strong wind stress lateral gradient, thermodynamic processes can outweigh the negative effect of the mechanical damping and may actually result in a net powering of the mesoscale field [*Byrne et al.*, 2016].

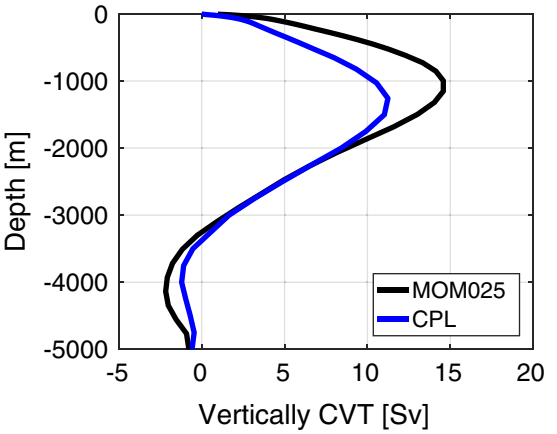

Figure 10. Meridional cumulative volume transport (CVT, in Sv; 1 Sv ≡ 10^6 m^3 s^{-1}) as a function of depth at 35°S, averaged over the period 1990–1995. The blue line represents the CVT computed from RegCM-ES and the black line is the transport obtained by the global ocean model MOM025. Note that a change in slope results in a change in flow direction (e.g., a negative slope corresponds to northward transport).

The surface EKE from the standalone ocean model, the coupled regional model, and the model MOM025 used to prescribe the open boundary conditions for the regional model is shown Figure 11, together with satellite observations for the period 1988–1997. Increased resolution in the ocean component improves the location of the Brazil-Malvinas confluence and produces a more energetic region compared to the relatively coarse global model. The region of influence of the Agulhas System is also better

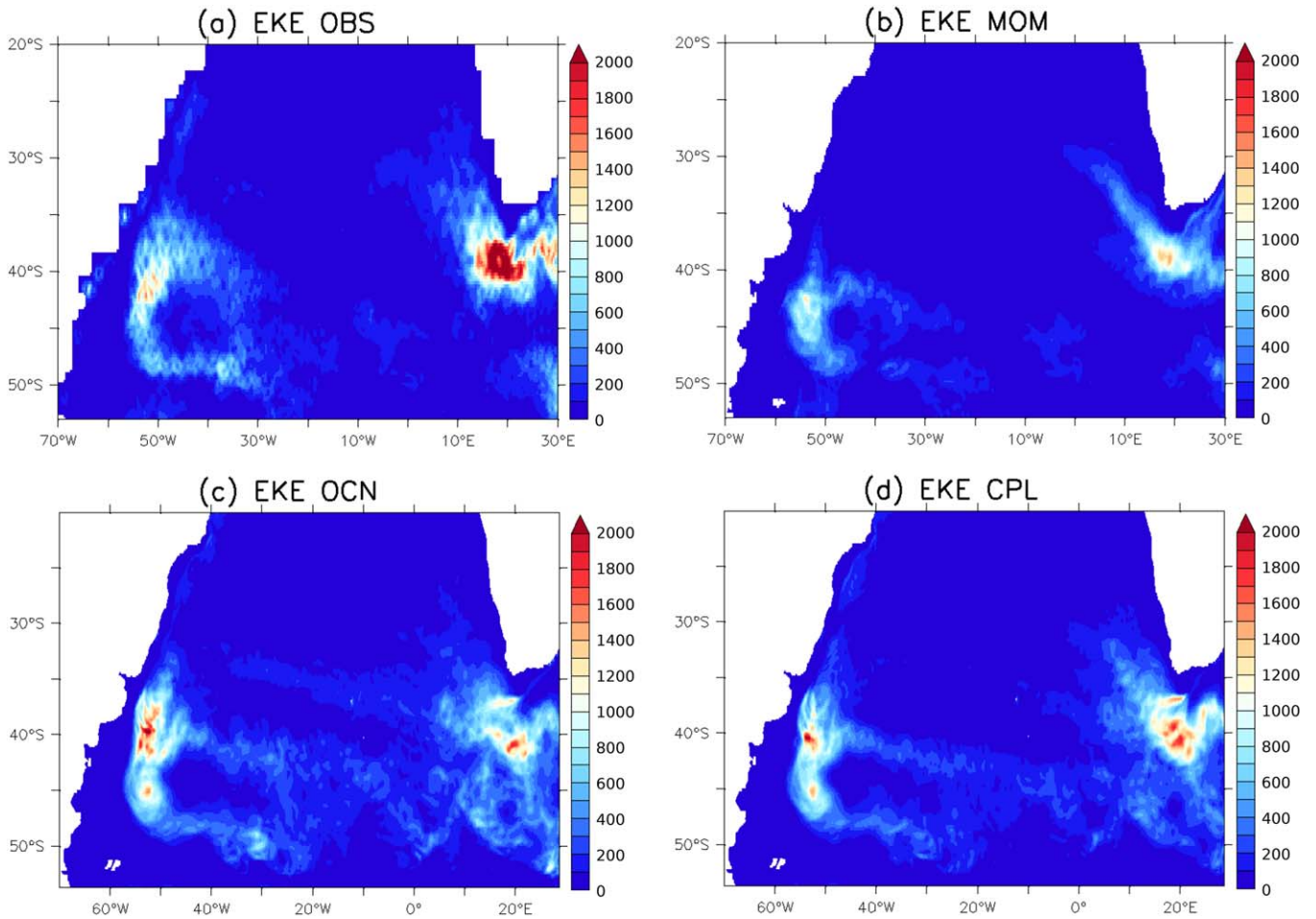

Figure 11. (a) Eddy kinetic energy (EKE) in (cm^{-2} s^{-2}) derived from satellite observations; (b) EKE obtained using the total velocity field from the global model MOM025; (c) standalone ocean model; and (d) coupled model. EKE is computed as a time-mean for the period 1988–1997.

represented with the regional models. Coupling to the atmosphere reduces the EKE in the Brazil-Malvinas confluence and increases EKE over the Agulhas retroflection resulting in values closer to observations. The mechanism of ocean-atmosphere interactions at the mesoscale is complex and requires a dedicated analysis for each region; however, these preliminary results show that ocean-atmosphere interactions are important and should be considered for a correct representation of the air-sea energy transfer.

Frontal regions like those in the Brazil-Malvinas confluence and the Agulhas current have been shown to induce a local forcing to the atmosphere, as SST fronts can modify the MABL trough changes in air-sea heat fluxes. Over colder (warmer) water, decreased (increased) surface heat fluxes stabilize (destabilize) the MABL, inhibiting (enhancing) the vertical turbulent mixing of momentum from aloft to the surface, increasing (reducing) the near-surface wind shear, and decelerating (accelerating) the surface winds. This SST influence on surface winds has been identified by means of satellite and in situ observations [*Jury*, 1994; *Rouault and Lutjeharms*, 2000; *Thum et al*., 2002; *Xie*, 2004; *Chelton et al*., 2004; *O'Neill et al*., 2003; *White and Annis*, 2003; *O'Neill et al*., 2005; *Tokinaga et al*., 2005; *Small et al*., 2008; *Chelton and Xie*, 2010; *O'Neill*, 2012], and analyzed in numerical studies [*Byrne et al*., 2016; *Xu and Xu*, 2015; *Kilpatrick et al*., 2016].

Figure 12 shows time-mean SST isolines (solid black lines) and wind speed (m s^{-1}) (left), wind divergence (10^{-6} s^{-1}) (center) and rainfall (mm d^{-1}) (right) over the Brazil-Malvinas Confluence region. RegCM-ES clearly shows air-sea coupling on annual mean conditions over the Brazil-Malvinas Confluence confirming the results of *Tokinaga et al*. [2005]. Over the cold Malvinas current winds are weaker, whereas they are intensified over the warm Brazil current, generating a strong surface wind divergence at the front. This is consistent with the SST-induced vertical mixing mechanism for wind adjustment. Moreover, rainfall is seen

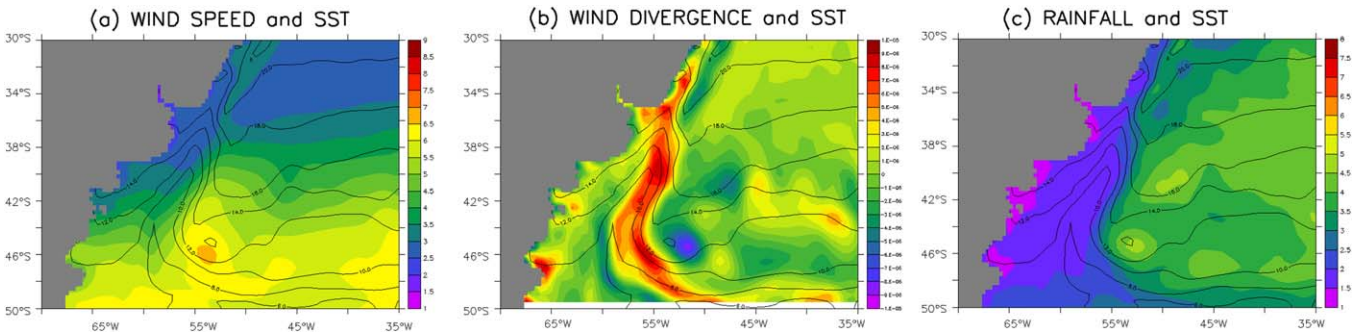

Figure 12. (a) Time-mean wind speed (m/s), (b) wind divergence (10^{-6} s^{-1}), and (c) rainfall (mm d^{-1}), for the Brazil-Malvinas Confluence region. Solid black lines represent SST isolines (contour interval is 2°C).

to increase substantially over the warm side of the front, with maxima over wind convergence (Figure 12). Similarly to previous results based on fine-resolution satellite measurements [*O'Neill et al*., 2003, 2005], RegCM-ES shows a strong convergence of surface winds surrounded by net divergence in the Agulhas Retroflection Current (Figure 13), resulting in increased rainfall over this warm current.

3.3. The Tropical Band

The atmospheric component RegCM4 can be run in a tropical band configuration referred to as the RegT-Band [*Coppola et al*., 2011]. This tropical band domain has also been tested with RegCM-ES. To the best of our knowledge, this is the first attempt at producing a fully coupled tropical channel model. Indeed, tropical regions exhibit intense air-sea interactions at all timescales (ENSO, intraseasonal atmospheric variations and their interactions with SSTs, to name a few) and coupled ocean-atmosphere dynamics can substantially benefit from the increased resolution achievable with a regional tropical band model compared to a global one.

The RegT-Band atmosphere domain extends from 43°N to 43°S and covers the entire tropical band in the longitudinal direction. The model uses a horizontal grid spacing of ∼100 km and 23 vertical levels. The initial and lateral boundary conditions are provided by the ERA-Interim reanalysis [*Dee et al*., 2011], where the atmosphere is not in contact with the dynamic ocean component, SST is also prescribed from Era-Interim reanalysis. In this configuration, we use the University of Washington Planetary Boundary Layer (UW-PBL) scheme [*Bretherton et al*., 2004], the *Tiedtke* [1989] cumulus convection scheme for both land and ocean, and the NT microphysics cloud scheme *Nogherotto et al*. [2016].

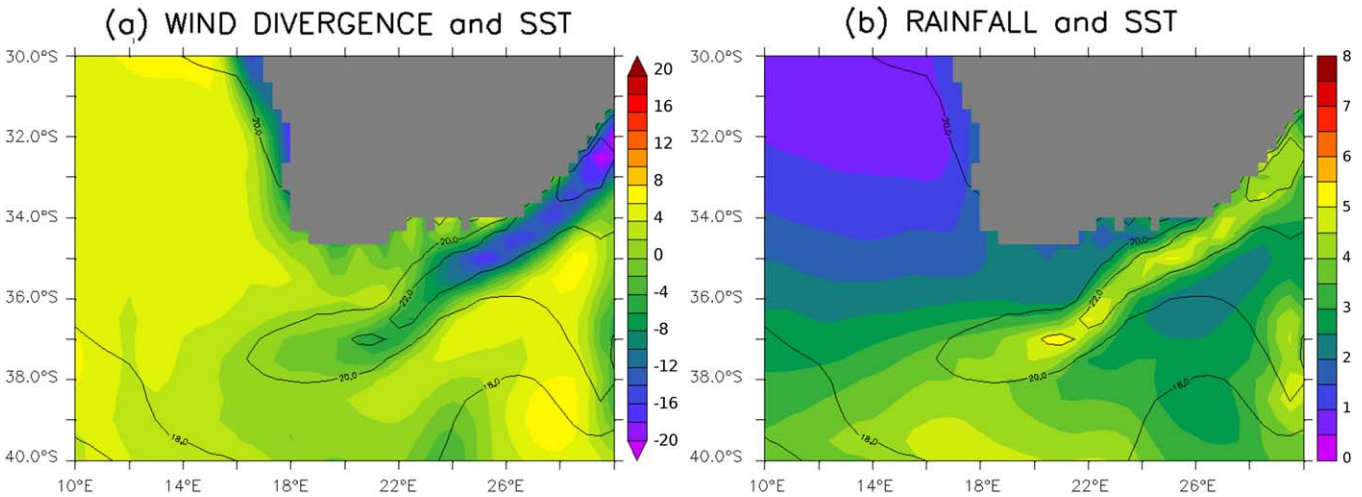

Figure 13. (a) Time-mean wind divergence (10^{-6} s^{-1}) and (b) rainfall (mm d^{-1}) over the region of the Agulhas System. Solid black lines represent the SST isolines (contour interval is 2°C).

The ocean component covers the tropical oceans from 30°N to 30°S. The horizontal resolution is 0.25° with 45 uneven vertical levels and the model employs the K-profile vertical mixing parameterization of *Large et al*. [1994]. The ocean started at rest, with temperature and salinity initial conditions taken from SODA reanalysis version 2.2.4 [*Carton and Giese*, 2008]. Lateral boundary conditions for velocities, temperature, and salinity are also imposed from SODA. The RegT-Band coupled simulation was run for 30 years, from 1979 to 2008.

The DJF and JJA precipitation climatologies in the coupled model are compared to the Global Precipitation Climatology Project (GPCP) precipitation data set [*Huffman et al*., 2001] in Figure 14. Results from the coupled model are comparable to the atmosphere-only simulations of *Coppola et al*. [2011] (not shown). The ITCZ location is correctly reproduced in both the Atlantic and Pacific Oceans, although a double ITCZ appears over the Pacific Ocean in both seasons and the precipitation intensity is slightly overestimated there. Despite an overestimation of the precipitation over the Indian Ocean in DJF, the Indian monsoon JJA climatology is well represented both over land and ocean. The same is found for the Indochina monsoon band and for the Western African monsoon. Further, if we focus on the South American monsoon DJF climatology, both the location and precipitation intensity over the Amazon and the Eastern Brazilian coast are consistent with observations.

In addition to the precipitation climatology, having a fully coupled ocean-atmosphere system in the tropical region calls for a verification of its ability to reproduce the observed SST interannual variability. In Figure 15, the SST annual standard deviation is shown for the coupled RegT-Band and the HadISST observational data set. The ENSO signal is evident in the coupled model, although weaker than observed. However, if we compute the Niño 3.4 anomaly index (5°S–5°N and 170–120°W) we see that the interannual variability of ENSO is well reproduced (Figure 16), even if the strength of the anomaly is generally underestimated.

This preliminary illustrative analysis shows that the coupled version of the RegT-Band is able to represent the tropical precipitation climatology along with its interannual variability over the tropical regions, with biases and weaknesses that are comparable to CMIP5-type coupled models [*Wang et al*., 2014]. A more in depth analysis of the coupled RegT-Band run is needed to fully evaluate this model configuration, but this requires a separate targeted study, which is currently under way. We also plan to refine the resolution of both ocean and atmosphere components, and to identify the best settings in order to reduce the remaining biases in the climatological mean state and variability.

4. Ongoing Developments

4.1. Hydrological Component: The ChyM Model

The main reason to include a new hydrological model in RegCM-ES is to allow the possibility to take into account also small river basins and finer scale spatial resolutions of river network than available in the 0.5° global grid of the HD model. A finer river network grid is needed in some particular domains highly affected by river discharge, as is the case of the Mediterranean Sea and Indian Ocean. One model that is suitable for this task is Cetemps Hydrological Model (CHyM) [*Coppola et al*., 2007], a spatially distributed hydrological model that uses a cellular automata algorithm to extract from a Digital Elevation Model (DEM) an eight flow direction map (D8). The model is able to simulate surface runoff, infiltration, evapotranspiration, percolation, melting, and return flow.

The initial aim of the CHyM model was to provide a general purpose tool for flood alert mapping which can be used for any geographical domain with any resolution allowed by the DEM, namely about 30 m in the current implementation. In previous applications, the model has been used to simulate climate change impacts on water resources in the Po river drainage basin, using offline coupling with two Regional Climate Models [*Coppola et al*., 2014].

An ad-hoc version of CHyM has been coupled to the Community Land Model 4.5 (CLM4.5) used in RegCM4 (see section 2). CLM4.5 provides the total runoff at each model grid point, which is then routed through each CHyM grid cell using a continuity and a momentum equation based on the kinematic wave approximation [*Lighthill and Whitham*, 1955] of the shallow water wave. In this approximation, the water flow velocity is a function of the longitudinal bed slope of the flow element, the Manning's roughness coefficient, and the hydraulic radius.

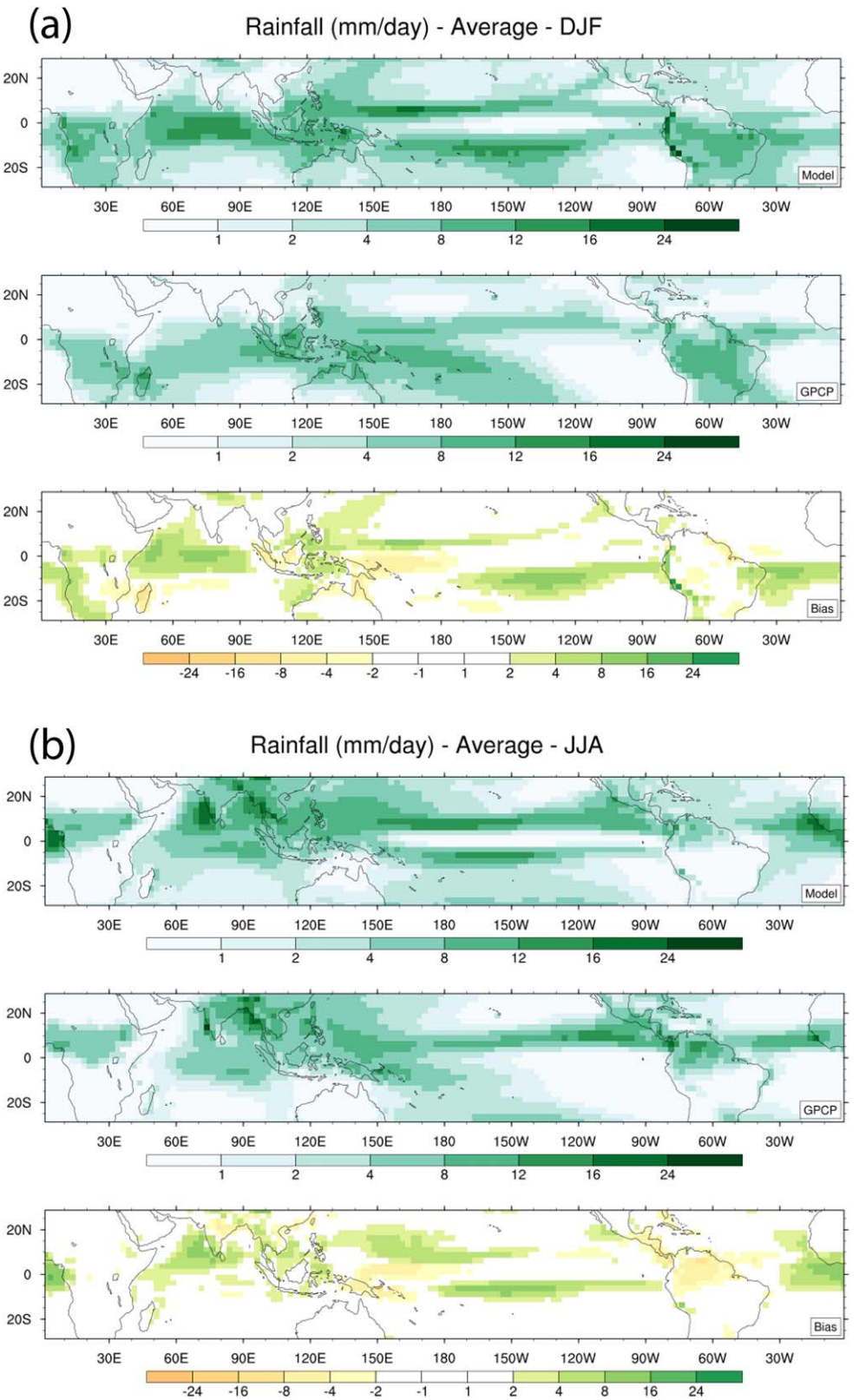

Figure 14. (a) DJF and (b) JJA precipitation climatologies from the coupled model, the Global Precipitation Climatology Project (GPCP), and relative biases. Climatologies are computed for the period 1979–2008.

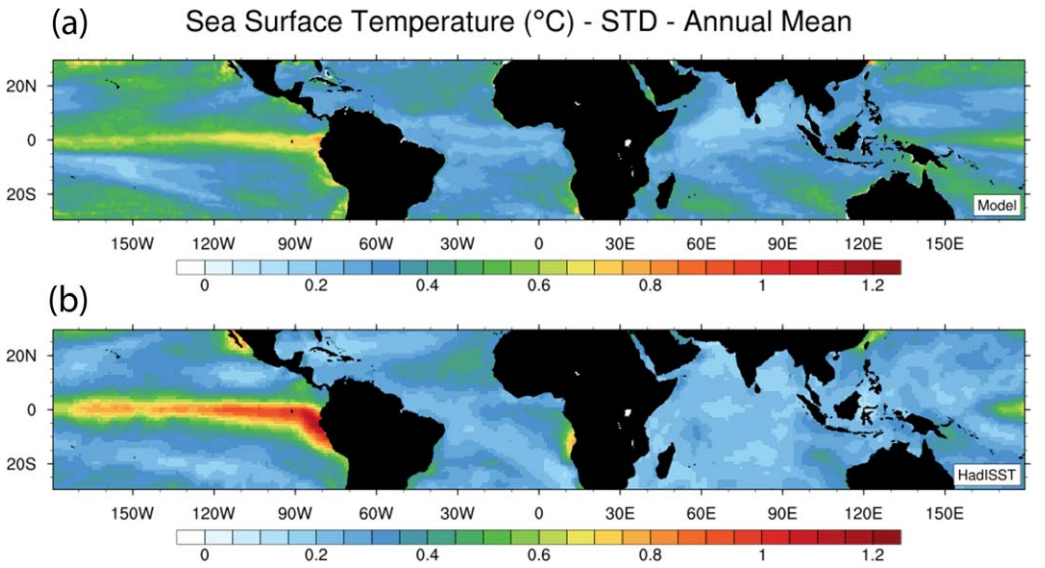

Figure 15. Annual-mean standard deviation (STD) of sea surface temperature for (a) the coupled RegCM-ES model and (b) the HadISST reanalysis, computed over the period 1979–2008.

In the preprocessing, CHyM builds the drainage networks at the selected domain and resolution (flow direction matrix, drained area, acclivity matrix, and Land Use map derived from United States Geological Surveys (USGS) products and scaled at the CHyM grid resolution). At run time, a velocity matrix is calculated taking into account the overland and channel flow, and the routing equations are integrated using a time step that depends on the spatial resolution used. The discharge values calculated at the river mouths are then interpolated and passed to the ocean during the run time. Furthermore, it is possible to select a threshold (defined as the minimum drained area by a mouth point) to discriminate rivers that have a very small catchment. The coupled RegCM-ES using the hydrological model CHyM is currently under testing and assessment for the South Asia CORDEX domain, as reported in a dedicated study [*Di Sante et al.*, 1993].

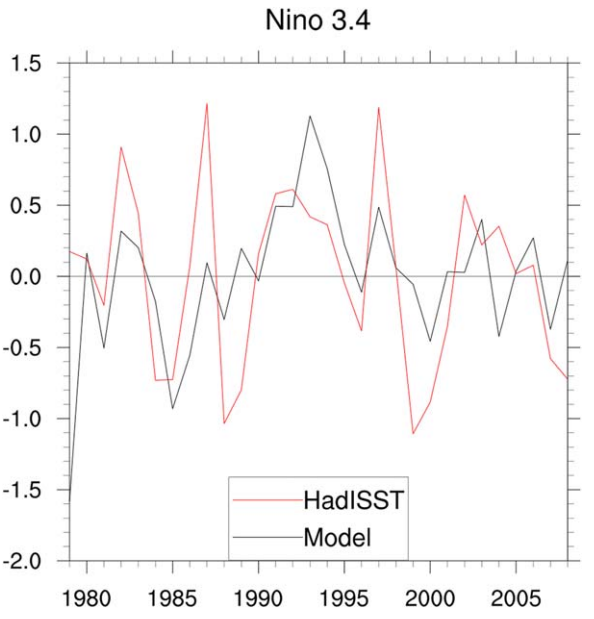

Figure 16. Time series of Nino3.4 index for the coupled model and the HadISST reanalysis.

4.2. Biogeochemical Component: The BFM Model

The latest implementation in RegCM-ES is the coupling with the ocean Biogeochemical Flux Model (BFM) [*Vichi et al.*, 2007a, 2007b, 2015]. BFM is a community model for the simulation of the dynamics of the main biogeochemical processes occurring in the marine ecosystems. It describes plankton dynamics and the cycles of carbon, phosphorus, nitrogen, silica, and oxygen in water. The model also describes seawater pH and carbonate dynamics, and it computes fluxes of CO_2 and oxygen at the air-sea interface. The code and the full description of the model equations and parameterizations are freely available at http://bfm-community.eu. BFM has been coupled with several ocean models and applied to the study of biogeochemical processes at the global [*Vichi et al.*, 2007b], regional [*Lazzari et al.*, 2012], and coastal scales [*Lamon et al.*, 2014]. Applications so far have included the study of the dynamics

of nitrate and phosphate [*Lazzari et al*., 2016], the assessment of ocean pH and alkalinity [*Cossarini et al*., 2015], and the quantification of marine sequestration of atmospheric carbon [*Canu et al*., 2015].

Simulations of RegCM-ES using BFM are currently been analyzed for the Mediterranean CORDEX domain using the same configuration adopted in *Cossarini et al*. [2016]. Preliminary results indicate that all major features of Mediterranean biogeochemistry are properly represented both spatially and temporally. The physical and biogeochemical performance of RegCM-ES in the Mediterranean basin will be presented in a follow-up study.

5. Conclusions

In this paper, we have described the development of a new Regional Earth System Model, RegCM-ES, and presented some illustrative tests of its physical performance over three limited domains. In order to provide a general, modular, extensible, and flexible tool that aims to support multiple model components and applications, RegCM-ES uses a driver based coupling approach [*Turuncoglu and Sannino*, 2016] currently supporting the coupling between the atmosphere, ocean, and land surface components. The regional coupled model also includes a hydrology and ocean biogeochemistry model.

Building on the community regional modeling system RegCM, RegCM-ES is an open source community model, making it suitable for use by a large scientific community on any regional domain of interest. RegCM-ES has already been successfully tested over some of the COordinated Regional Downscaling Experiment (CORDEX) domains, namely the Mediterranean, South Asia, and Central America domains, and additional domains such as the South Atlantic and the Tropical Band (Figure 3).

A comparison between atmosphere-only and coupled simulations with RegCM-ES, together with sensitivity tests to different physical parameterizations, have shown good indications toward improving the simulation of various physical climate characteristics in regions where coupled air-sea processes and interactions are important. For example, in the illustrative cases, we discussed here, compared to the standalone atmospheric counterpart, RegCM-ES showed a reduction of precipitation biases and a better location of the ITCZ over the North Atlantic and Caribbean Sea (Central America domain). The coupled Tropical Band configuration also showed a realistic and often improved representation of the ITCZ and monsoon climatologies [see *Coppola et al*., 2011], along with a realistic representation of ENSO variability (although with underestimated magnitude). On the ocean side, oceanic meridional fluxes, partly constrained by the lateral conditions, were well reproduced by the RegCM-ES model. The coupled model also showed an encouraging performance in simulating the effects of air-sea interactions, as for example shown for the case of the Agulhas and the Brazil-Malvinas systems [*Tokinaga et al*., 2005; *O'Neill et al*., 2003, 2005].

The open-source coupled model will undergo a continuous development and testing—also thanks to the large RegCNET community [*Giorgi and Anyah*, 2012]—including future improvements on its dynamics [*Tumolo et al*., 2013; *Tumolo and Bonaventura*, 2015] and updates on existing components (e.g., RegCM4, MITgcm, CHym, CLM, BFM). Clearly, the RegCM-ES system needs to be further assessed over different domains and for a wide range of applications. Therefore, we encourage interested users to access the model code, extensively test it for different scientific problems and possibly contribute to its development.

Acknowledgments
L. Sitz acknowledges funding from the Programme for Training and Research in Italian Laboratories (TRIL) program of the Abdus Salam International Centre for Theoretical Physics (ICTP). M. Reale was supported by OGS and CINECA under the HPC Training and Research for Earth Sciences (HPC-TRES) program award 2015–07. GPCP Precipitation data provided by the NOAA/OAR/ESRL PSD, Boulder, Colorado, USA, from their web site at http://www.esrl.noaa.gov/psd/. NOAA NCDC ERSST data are available from https://www.ncdc.noaa.gov/data-access/marineocean-data/extended-reconstructed-sea-surface-temperature-ersst. All data used are available on the storage system at ICTP and can be obtained on request (rfarneti@ictp.it).

References

Artale, V., et al. (2010), An atmosphere-ocean regional climate model for the Mediterranean area: Assessment of a present climate simulation, *Clim. Dyn.*, *35*(5), 721–740.

Baringer, M., and S. Garzoli (2007), Meridional heat transport determined with expendable bathythermographs—Part I: Error estimates from model and hydrographic data, *Deep Sea Res., Part I*, *54*, 1390–1401.

Barreiro, M., P. Chang, and R. Saravana (2002), Variability of the South Atlantic convergence zone as simulated by an atmospheric general circulation model, *J. Clim.*, *15*, 745–763.

Barreiro, M., P. Chang, and R. Saravanan (2005), Simulated precipitation response to SST forcing and potential predictability in the region of the South Atlantic convergence zone, *Clim. Dyn.*, *24*, 105–114, doi:10.1007/s00382-004-0487-9.

Bender, M. A., I. Ginis, and Y. Kurihara (1993), Numerical simulations of tropical cyclone-ocean interaction with a high-resolution coupled model, *J. Geophys. Res.*, *98*, 23,245–23,263.

Brand, S. (1971), The effects on a tropical cyclone of cooler surface waters due to upwelling and mixing produced by a prior tropical cyclone, *J. Appl. Meteorol.*, *10*, 865–874.

Bretherton, C. S., J. R. McCaa, and H. Grenier (2004), A new parameterization for shallow cumulus convection and its application to marine subtropical cloud-topped boundary layers. Part I: Description and 1d results, *Mon. Weather Rev.*, *132*, 864–882.

Byrne, D., M. Münnich, I. Frenger, and N. Gruber (2016), Mesoscale atmosphere ocean coupling enhances the transfer of wind energy into the ocean, *Nat. Commun.*, *7*, 11,867, doi:10.1038/ncomms11867.
Canu, D., A. Ghermandi, P. Nunes, P. Lazzari, G. Cossarini, and C. Solidoro (2015), Estimating the value of carbon sequestration ecosystem services in the Mediterranean Sea: An ecological economics approach, *Global Environ. Change*, *32*, 87–95.
Carton, J., and B. Giese (2008), A reanalysis of ocean climate using simple ocean data assimilation (SODA), *Mon. Weather Rev.*, *136*, 2999–3017, doi:10.1175/2007MWR1978.1.
Chelton, D., M. Schlax, M. Freilich, and R. Milliff (2004), Satellite measurements reveal persistent small-scale features in ocean winds, *Science*, *303*, 978–983, doi:10.1126/science.1091901.
Chelton, D. B., and S. Xie (2010), Coupled ocean-atmosphere interaction at oceanic mesoscales, *Oceanography*, *23*, 52–69, doi:10.5670/oceanog.2010.05.
Collins, N., G. Theurich, C. DeLuca, M. Suarez, A. Trayanov, V. Balaji, P. Li, W. Yang, C. Hill, and A. da Silva (2005), Design and implementation of components in the Earth System Modeling Framework, *Int. J. High Perform. Comput. Appl.*, *19*(3), 341–350.
Coppola, E., B. Tomasetti, L. Mariotti, M. Verdecchia, and G. Visconti (2007), Cellular automata algorithms for drainage network extraction and rainfall data assimilation, *Hydrol. Sci. J.*, *52*, 579–592.
Coppola, E., F. Giorgi, L. Mariotti, and X. Bi (2011), RegT-Band: A tropical band version of RegCM4, *Clim. Res.*, *52*, 115–133.
Coppola, E., M. Verdecchia, F. Giorgi, V. Colaiuda, B. Tomassetti, and A. Lombardi (2014), Changing hydrological conditions in the Po basin under global warming, *Sci. Total Environ.*, *493*, 1183–1196.
Cossarini, G., P. Lazzari, and C. Solidoro (2015), Spatiotemporal variability of alkalinity in the Mediterranean Sea, *Biogeosciences*, *12*(6), 1647–1658.
Cossarini, G., S. Querin, C. Solidoro, G. Sannino, P. Lazzari, V. Di Biagio, and G. Bolzon (2016), Development of BFMCOUPLER (v1.0), the coupling scheme that links the MITgcm and BFM models for ocean biogeochemistry simulations, *Geosci. Model Dev.*, *10*, 1423–1445, doi:10.5194/gmd-2016-222.
Danabasoglu, G., et al. (2014), North Atlantic simulations in Coordinated Ocean-ice Reference Experiments phase II (CORE-II): Part I: Mean states, *Ocean Modell.*, *73*, 76–107.
Dare, R., and J. McBride (2011), Sea surface temperature response to tropical cyclones, *Mon. Weather Rev.*, *139*(12), 3798–3808.
da Rocha, R., S. Cuadra, M. Reboita, L. Kruger, T. Ambrizzi, and N. Krusche (2012), Effects of RegCM3 parameterizations on simulated rainy season over South America, *Clim. Res.*, *52*, 253–265, doi:10.3354/cr01065.
Dee, D. P., et al. (2011), The ERA-Interim reanalysis: Configuration and performance of the data assimilation system, *Q. J. R. Meteorol. Soc.*, *137*, 553–597.
Dickinson, R. E., A. Henderson-Sellers, and P. J. Kennedy (1993), *Biosphere-atmosphere Transfer Scheme (BATS) Version 1e as Coupled to the NCAR Community Climate Model*, NCAR Technical Note NCAR/TN-387+STR, doi:10.5065/D67W6959.
Dong, S., S. Garzoli, M. Baringer, C. Meinen, and G. Goni (2009), Interannual variations in the Atlantic meridional overturning circulation and its relationship with the net northward heat transport in the South Atlantic, *Geophys. Res. Lett.*, *36*, L20606, doi:10.1029/2009GL039356.
Dong, S., S. Garzoli, and M. Baringer (2011), The role of interocean exchanges on decadal variations of the meridional heat transport in the South Atlantic, *J. Phys. Oceanogr.*, *41*, 1498–1511, doi:10.1175/2011JPO4549.1.
Emanuel, K. (1991), A scheme for representing cumulus convection in large scale models, *J. Atmos. Sci.*, *48*, 2313–2335.
Emanuel, K. (2001), Contribution of tropical cyclones to meridional heat transport by the oceans, *J. Geophys. Res.*, *106*, 14,771–14,781.
Fuentes-Franco, R., E. Coppola, F. Giorgi, F. Graef, and E. Pavia (2014), Assessment of RegCM4 simulated inter-annual variability and daily-scale statistics of temperature and precipitation over Mexico, *Clim. Dyn.*, *42*, 629–647.
Fuentes-Franco, R., F. Giorgi, E. Coppola, and K. Zimmermann (2016), Sensitivity of tropical cyclones to resolution, convection scheme and ocean flux parameterization over Eastern Tropical Pacific and Tropical North Atlantic Oceans in the RegCM4 model, *Clim. Dyn.*, *49*, 547–561, doi:10.1007/s00382-016-3357-3.
Furue, R., Y. Jia, J. P. McCreary, N. Schneider, K. J. Richards, P. Muller, B. D. Cornuelle, N. Martinez Avellaneda, D. Stammer, C. Liu, and A. Kohl (2015), Impacts of regional mixing on the temperature structure of the equatorial Pacific Ocean. Part 1: Vertically uniform vertical diffusion, *Ocean Modell.*, *91*, 91–111.
Giorgi, F., and R. Anyah (2012), The road towards RegCM4, *Clim. Res.*, *52*, 3–6.
Giorgi, F., M. R. Marinucci, G. Bates, and G. DeCanio (1993), Development of a second generation regional climate model (RegCM2): II. Convective processes and assimilation of lateral boundary conditions, *Mon. Weather Rev.*, *121*, 2814–2832.
Giorgi, F., C. Jones, and G. Asrar (2009), Addressing climate information needs at the regional level: The CORDEX framework, *World Meteorol. Organ Bull.*, *58*, 175–183.
Giorgi, F., et al. (2012), RegCM4: Model description and preliminary tests over multiple CORDEX domains, *Clim. Res.*, *52*, 7–29.
Grell, G. A., J. Dudhia, and D. Stauffer (1994), A description of the fifth-generation Penn State/NCAR Mesoscale Model (MM5), NCAR Technical Note NCAR/TN-398+STR, doi:10.5065/D60Z716B.
Griffies, S., and R. Hallberg (2000), Biharmonic friction with a Smagorinsky-like viscosity for use in large-scale eddy-permitting ocean models, *Mon. Weather Rev.*, *128*(8), 2935–2946.
Griffies, S., A. Biastoch, C. Boning, F. Bryan, G. Danabasoglu, E. Chassignet, M. England, R. Gerdes, H. Haak, and R. Hallberg (2009), Coordinated ocean-ice reference experiments (CORES), *Ocean Modell.*, *26*(1–2), 1–46.
Hagemann, S., and L. Dümenil (1998), A parameterization of the lateral waterflow for the global scale, *Clim. Dyn.*, *14*, 17–31.
Hagemann, S., and L. Dümenil (2001), Validation of the hydrological cycle of ECMWF and NCEP reanalyses using the MPI hydrological discharge model, *J. Geophys. Res.*, *106*, 1503–1510.
Hart, R. E. (2011), An inverse relationship between aggregate Northern Hemisphere tropical cyclone activity and subsequent winter climate, *Geophys. Res. Lett.*, *38*, L01705, doi:10.1029/2010GL045612.
Hart, R. E., R. N. Maue, and M. C. Watson (2007), Estimating local memory of tropical cyclones through MPI anomaly evolution, *Mon. Weather Rev.*, *135*, 3990–4005.
Hill, C., C. DeLuca, V. Balaji, M. Suarez, and A. Da Silva (2004a), The architecture of the earth system modeling framework, *Comput. Sci. Eng.*, *6*(1), 18–28, doi:10.1109/MCISE.2004.1255817.
Hill, C., et al. (2004b), Implementing applications with the earth system modeling framework, *Lect. Notes Comput. Sci.*, *3732*, 563–572.
Hostetler, S., G. Bates, and F. Giorgi (1993), Interactive nesting of a lake thermal model within a regional climate model for climate change studies, *J Geophys. Res.*, *98*, 5045–5057.
Huffman, G., R. Adler, M. Morrissey, D. Bolvin, S. Curtis, R. Joyce, B. McGavock, and J. Susskind (2001), Global precipitation at one-degree daily resolution from multisatellite observations, *J. Hydrometeorol.*, *2*, 36–50.
Jansen, M. F., R. Ferrari, and T. A. Mooring (2010), Seasonal versus permanent thermocline warming by tropical cyclones, *Geophys. Res. Lett.*, *37*, L03602, doi:10.1029/2009GL041808.

Jury, M. (1994), A thermal front within the marine atmospheric boundary layer over the Agulhas Current South of Africa: Composite aircraft observations, *J. Geophys. Res.*, *99*, 3297–3304.
Kiehl, J., J. Hack, G. Bonan, B. Boville, B. Briegleb, D. Williamson, and P. Rasch (1996), Description of the NCAR community climate model (CCM3), *Tech. Rep. TN-420+STR*, Natl. Cent. for Atmos. Res., Boulder, Colo.
Kilpatrick, T., N. Schneider, and B. Qiu (2016), Atmospheric Response to a Midlatitude SST Front: Alongfront Winds, *J. Atmos. Sci.*, *73*, 3489–3509, doi:10.1175/JAS-D-15-0312.1.
Lamon, L., et al. (2014), An ensemble of models for identifying climate change scenarios in the Gulf of Gabes, Tunisia, *Reg. Environ. Change*, *14*, 31–40, doi:10.1007/s10113-013-0430-x.
Large, W., J. C. McWilliams, and S. C. Doney (1994), Oceanic vertical mixing: A review and a model with a nonlocal boundary layer parameterization, *Rev. Geophys.*, *32*(4), 363–403, doi:10.1029/94RG01872.
Lazzari, P., C. Solidoro, V. Ibello, S. Salon, A. Teruzzi, E. K. Bérang, S. Colella, and A. Crise (2012), Seasonal and inter-annual variability of plankton chlorophyll and primary production in the Mediterranean Sea: A modelling approach, *Biogeosciences*, *9*, 217–233, doi:10.5194/bg-9-217-2012.
Lazzari, P., C. Solidoro, S. Salon, and G. Bolzon (2016), Spatial variability of phosphate and nitrate in the Mediterranean Sea: A modeling approach, *Deep Sea Res., Part I*, *108*, 39–52.
Leipper, D. F. (1967), Observed ocean conditions and hurricane Hilda, 1964, *J. Atmos. Sci.*, *24*, 182–196.
Lighthill, M. J., and C. B. Whitham (1955), On kinematic waves. I. Flood movement in long rivers, *Proc. R. Soc. A*, *229*, 281–316.
Lin, I., W. T. Liu, C.-C. Wu, G. T. F. Wong, C. Hu, Z. Chen, W.-D. Liang, Y. Yang, and K.-K. Liu (2003), New evidence for enhanced ocean primary production triggered by tropical cyclone, *Geophys. Res. Lett.*, *30*(13), 1718, doi:10.1029/2003GL017141.
Marshall, J., A. Adcroft, C. Hill, L. Perelman, and C. Heisey (1997), A finite-volume, incompressible Navier-Stokes model for studies of the ocean on parallel computers, *J. Geophys. Res.*, *102*, 5753–5766.
Misra, V., S. Chan, R. Wu, and E. Chassignet (2009), Air-sea interaction over the Atlantic warm pol in the NCEP CFS, *Geophys. Res. Lett.*, *36*, L15702, doi:10.1029/2009GL038737.
Nogherotto, R., A. M. Tompkins, G. Giuliani, E. Coppola, and F. Giorgi (2016), Numerical framework and performance of the new multiple-phase cloud microphysics scheme in RegCM4.5: Precipitation, cloud microphysics, and cloud radiative effects, *Geosci. Model Dev.*, *9*, 2533–2547, doi:10.5194/gmd-9-2533-2016.
Oleson, K. W., and Coauthors (2010), *Technical Description of version 4.0 of the Community Land Model (CLM)*, NCAR Technical Note NCAR/TN-478+STR, doi:10.5065/D6FB50WZ.
O'Neill, L. (2012), Wind speed and stability effects on coupling between surface wind stress and SST observed from buoys and satellite, *J. Clim.*, *25*, 1544–1569, doi:10.1175/JCLI-D-11-00121.1.
O'Neill, L., D. Chelton, and S. Esbensen (2003), Observations of SST-induced perturbations of the wind stress field over the Southern Ocean on seasonal time scales, *J. Clim.*, *26*, 2340–2354.
O'Neill, L., D. Chelton, and S. Esbensen (2005), High-resolution satellite measurements of the atmospheric boundary layer response to SST variations along the Agulhas Return Current, *J. Clim.*, *18*, 2706–2723.
O'Neill, L., S. Esbensen, N. Thum, R. Samelson, and D. Chelton (2010), Dynamical analysis of the boundary layer and surface wind responses to mesoscale SST perturbations, *J. Clim.*, *23*, 559–581, doi:10.1175/2009JCLI2662.1.
O'Neill, L. W., D. B. Chelton, and S. K. Esbensen (2012), Covariability of surface wind and stress responses to sea surface temperature fronts, *J. Clim.*, *25*, 5916–5942, doi:10.1175/JCLI-D-11-00230.1.
Pal, J., E. Small, and E. Eltahir (2000), Simulation of regional-scale water and energy budgets: Representation of subgrid cloud and precipitation processes within RegCM, *J. Geophys. Res.*, *105*, 29,579–29,594.
Perez, R., S. Garzoli, C. Meinen, and R. Matano (2011), Geostrophic velocity measurement techniques for the meridional overturning circulation and meridional heat transport in the South Atlantic, *J. Atmos. Oceanic Technol.*, *28*, 1504–1521, doi:10.1175/JTECH-D-11-00058.1.
Price, J. F. (1981), Upper ocean response to a hurricane, *J. Phys. Oceanogr.*, *11*, 153–175.
Price, J. F., J. Morzel, and P. P. Niiler (2008), Warming of SST in the cool wake of a moving hurricane, *J. Geophys. Res.*, *113*, C07010, doi:10.1029/2007JC004393.
Ratnam, J. V., F. Giorgi, A. Kaginalkar, and S. Cozzini (2009), Simulation of the Indian monsoon using the RegCM3-ROMS regional coupled model, *Clim. Dyn.*, *33*(1), 119–139.
Reale, M., A. Crise, R. Farneti, and R. Mosetti (2016), A process study of the Adriatic-Ionian system baroclinic dynamics, *J Geophys. Res.*, *121*, 5872—5887.
Reboita, M., J. Fernandez, M. Llopart, R. da Rocha, L. Pampuch, and F. Cruz (2014), Assessment of RegCM4.3 over the CORDEX South America domain: Sensitivity analysis for physical parameterization schemes, *Clim. Res.*, *60*, 215–234, doi:10.3354/cr01239.
Reynolds, R. W., T. M. Smith, C. Liu, D. Chelton, K. Casey, and M. Schlax (2007), Daily high-resolution-blended analyses for sea surface temperature, *J. Clim.*, *20*, 5473–5496.
Rosso, I., A. M. Hogg, A. E. Kiss, and B. Gayen (2015), Topographic influence on submesoscale dynamics in the Southern Ocean, *Geophys. Res. Lett.*, *42*, 1139–1147, doi:10.1002/2014GL062720.
Rouault, M., and J. Lutjeharms (2000), Air-sea exchange over an Agulhas eddy at the subtropical convergence, *Global Atmos. Ocean Syst.*, *7*, 125–150.
Rousset, C., and L. M. Beal (2010), Observations of the Florida and Yucatan currents from a Caribbean cruise ship, *J. Phys. Oceanogr.*, *40*, 1575–1581.
Rousset, C., and L. M. Beal (2011), On the seasonal variability of the currents in the straits of Florida and Yucatan Channel, *J. Geophys. Res.*, *116*, C08004, doi:10.1029/2010JCC006679.
Sannino, G., M. Hermann, A. Carillo, V. Rupolo, V. Ruggiero, V. Artale, and P. Heimbach (2009), An eddy-permitting model of the Mediterranean Sea with a two-way grid refinement at the Strait of Gibraltar, *Ocean Modell.*, *30*, 56–72.
Sannino, G., A. Carillo, G. Pisacane, and C. Naranjo (2015), On the relevance of tidal forcing in modelling the Mediterranean thermohaline circulation, *Prog. Oceanogr.*, *134*, 304–329.
Sein, D. V., U. Mickolajewicz, M. Groger, I. Fast, W. Cabos, J. G. Pinto, S. Hagemann, T. Semmler, A. Izquierdo, and D. Jacob (2015), Regionally coupled atmosphere-ocean-sea ice-marine biogeochemistry model ROM: 1. Description and validation, *J. Adv. Model. Earth Syst.*, *7*, 268–304, doi:10.1002/2014MS000357.
Seo, H., M. Jochum, R. Murtugudde, and A. J. Miller (2006), Effect of ocean mesoscale variability on the mean state of tropical Atlantic climate, *Geophys. Res. Lett.*, *33*, L09606, doi:10.1029/2005GL025651.
Seo, H., A. Miller, and J. Norris (2016), Eddy-wind interaction in the California current system: Dynamics and impacts, *J. Phys. Oceanogr.*, *46*, 439–459, doi:10.1175/JPO-D-15-0086.1.

Sitz, L., R. Farneti, and S. M. Griffies (2015), Simulated South Atlantic transports and their variability during 1958–2007, *Ocean Modell.*, *91*(2015), 70–90.
Sloyan, B., and S. Rintoul (2001), The Southern Ocean limb of the global deep overturning circulation, *J. Phys. Oceanogr.*, *31*, 143–173.
Smagorinsky, J. (1993), *Large Eddy Simulation of Complex Engineering and Geophysical Flows*, Cambridge Univ. Press, Cambridge, U. K.
Small, E. E., L. C. Sloan, S. Hostetler, and F. Giorgi (1999), Simulating the water balance of the Aral sea with a coupled regional climate-lake model, *J. Geophys. Res.*, *104*, 6583–6602.
Small, R. J., E. Curchitser, K. Hedstrom, B. Kauffman, and W. G. Large (2015), The benguela upwelling system: Quantifying the sensitivity to resolution and coastal wind representation in a global climate model, *J. Clim.*, *28*, 9409–9432, doi:10.1175/JCLI-D-15-0192.1.
Small, R. J., S. P. deSzoeke, S. Xie, L. O'Neill, H. Seo, Q. Song, P. Cornillon, M. Spall, and S. Minobe (2008), Air-sea interaction over the ocean fronts and eddies, *Dyn. Atmos. Oceans*, *45*, 274–319, doi:10.1016/j.dynatmoce.2008.01.001.
Smith, R. H. (2010), Atlantic-Caribbean exchange through Windward Passage, Master's thesis, Univ. of Miami, Coral Gables, Fla.
Smith, W. H. F., and D. T. Sandwell (1997), Global seafloor topography from satellite altimetry and ship depth soundings, *Science*, *277*, 1957–1962.
Solman, S., et al. (2013), Evaluation of an ensemble of regional climate model simulations over South America driven by the ERA-Interim reanalysis: Model performance and uncertainties, *Clim. Dyn.*, *41*, 1139, doi:10.1007/s00382-013-1667-2.
Solmon, F., V. S. Nair, and M. Mallet (2015), Increasing Arabian dust activity and the Indian summer monsoon, *Atmos. Chem. Phys.*, *15*, 8051–8064.
Stammer, D., C. Wunsch, R. Giering, C. Eckert, P. Heimbach, J. Marotzke, A. Adcroft, C. N. Hill, and J. Marshall (2003), Volume, heat, and freshwater transports of the global ocean circulation 1993–2000, estimated from a general circulation model constrained by World Ocean Circulation Experiment (WOCE) data, *J. Geophys. Res.*, *108*(C1), 3007, doi:10.1029/2001JC001115.
Talley, L. (2008), Freshwater transport estimates and the global overturning circulation: Shallow, deep and throughflow components, *Prog. Oceanogr.*, *78*, 257–303.
Thum, N., S. Esbensen, D. B. Chelton, and M. McPhaden (2002), Air-sea heat exchange along the northern sea surface temperature front in the eastern tropical Pacific, *J. Clim.*, *15*, 3361–3378.
Tiedtke, M. (1989), A comprehensive mass flux scheme for cumulus parameterization in large-scale models, *Mon. Weather Rev.*, *117*(8), 1779–1800.
Tirabassi, G., C. Masoller, and M. Barreiro (2014), A study of the air-sea interaction in the South Atlantic convergence zone through granger causality, *Int. J. Climatol.*, *35*, 3440–3453.
Tokinaga, H., Y. Tanimoto, and S. Xie (2005), SST-induced surface wind variations over the Brazil-Malvinas confluence: Satellite and in situ observations, *J. Clim.*, *18*, 3470–3482, doi:10.1175/JCLI3485.1.
Trenberth, K., and J. Fasullo (2007), Water and energy budgets of hurricanes and implications for climate change, *J. Geophys. Res.*, *112*, D23107, doi:10.1029/2006JD008304.
Tumolo, G., and L. Bonaventura (2015), A semi-implicit, semi-Lagrangian discontinuous Galerkin framework for adaptive numerical weather prediction, *Q. J. R. Meteorol. Soc.*, *141*, 2582–2601, doi:10.1002/qj.2544.
Tumolo, G., L. Bonaventura, and M. Restelli (2013), A semi-implicit, semi-Lagrangian, p-adaptive discontinuous Galerkin method for the shallow water equations, *J. Comput. Phys.*, *232*, 46–67.
Turuncoglu, U., and G. Sannino (2016), Validation of newly designed regional earth system model (RegESM) for Mediterranean basin, *Clim. Dyn.*, *48*, 2919–2947, doi:10.1007/s00382-016-3241-1.
Turuncoglu, U., G. Giuliani, N. Elguindi, and F. Giorgi (2013), Modelling the Caspian sea and its catchment area using a coupled regional atmosphere-ocean model (RegCM4-ROMS): Model design and preliminary results, *Geosci. Model Dev.*, *6*, 283–299.
Vichi, M., S. Masina, and A. Navarra (2007a), A generalized model of pelagic biogeochemistry for the global ocean ecosystem: Part II: Numerical simulations, *J. Mar. Syst.*, *64*, 110–134.
Vichi, M., N. Pinardi, and S. Masina (2007b), A generalized model of pelagic biogeochemistry for the global ocean ecosystem: Part I: Theory, *J. Mar. Syst.*, *64*, 89–109.
Vichi, M., et al. (2015), The biogeochemical flux model (BFM): Equation description and user manual, BFM version 5.1., BFM Report series N. 1, Release 1.1, August 2015, 104 pp., Bologna, Italy. [Available at http://bfm-community.eu.]
Walker, N. D., R. Leben, and S. Balasubramanian (2005), Hurricane-forced upwelling and chlorophyll a enhancement within cold-core cyclones in the Gulf of Mexico, *Geophys. Res. Lett.*, *32*, L18610, doi:10.1029/2005GL023716.
Wang, C., L. Zhang, S. K. Lee, L. Wu, and C. R. Mechoso (2014), A global perspective on CMIP5 climate model biases, *Nat. Clim. Change*, *4*(3), 201–205.
White, W., and J. Annis (2003), Coupling of extratropical mesoscale eddies in the ocean to westerly winds in the atmospheric boundary layer, *J. Phys. Oceanogr.*, *33*, 1095–1107.
Xie, S. (2004), Satellite observations of cool ocean-atmosphere interaction, *Bull. Am. Meteorol. Soc.*, *85*, 195–209, doi:10.1175/BAMS-85-2-195.
Xu, M., and H. Xu (2015), Atmospheric responses to Kuroshio SST front in the East China Sea under different prevailing winds in winter and spring, *J. Clim.*, *28*, 3191–3211, doi:10.1175/JCLI-D-13-00675.1.
Zeng, X., M. Zhao, and R. Dickinson (1998), Intercomparison of bulk aerodynamic algorithms for the computation of sea surface fluxes using TOGA COARE and TAO data, *J. Clim.*, *11*, 2628–2644.